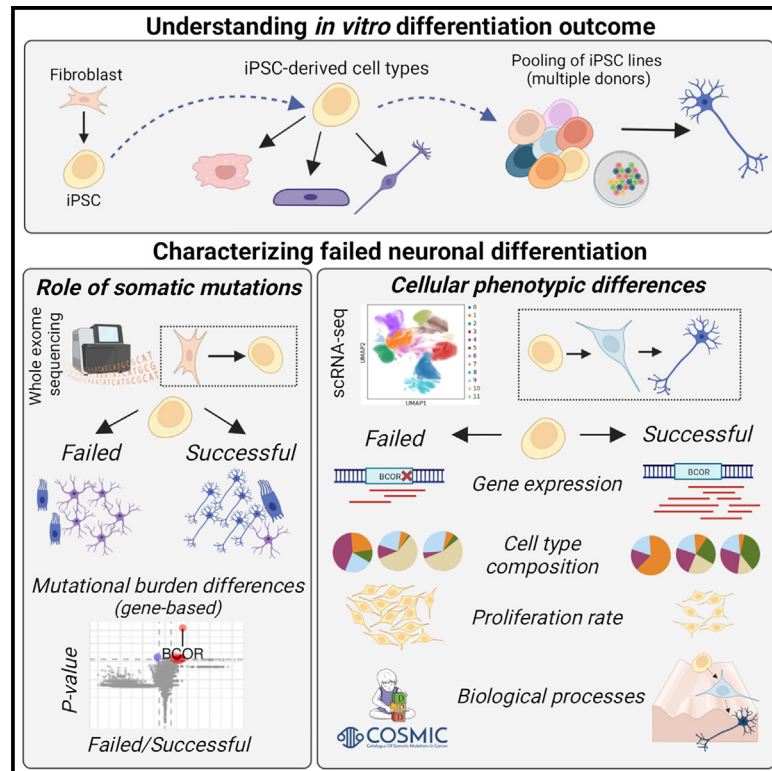


Somatic mutations alter the differentiation outcomes of iPSC-derived neurons

Graphical abstract



Authors

Pau Puigdevall, Julie Jerber, Petr Danecek, Sergi Castellano, Helena Kilpinen

Correspondence

pau.puigdevall@helsinki.fi (P.P.), helena.kilpinen@helsinki.fi (H.K.)

In brief

A remaining challenge in the use of iPSCs to study neurodevelopment is the variability of differentiation outcomes. Puigdevall et al. analyzed 238 iPSC lines and showed that those with deleterious somatic mutations in *BCOR* produce fewer neurons, proliferate faster, and undergo major early changes in cell type composition and gene expression.

Highlights

- Differentiation ability of individual iPSC lines is highly variable
- Somatic mutations' effects on differentiation outcome were evaluated in 238 iPSC lines
- Loss-of-function mutations in *BCOR* compromise the production of dopaminergic neurons
- Differentiation failure due to *BCOR* mutations is linked to increased proliferation



Article

Somatic mutations alter the differentiation outcomes of iPSC-derived neurons

Pau Puigdevall,^{1,4,*} Julie Jerber,² Petr Danecek,³ Sergi Castellano,^{1,6} and Helena Kilpinen^{1,3,4,5,6,7,*}¹UCL Great Ormond Street Institute of Child Health, University College London, 30 Guilford Street, London WC1N 1EH, UK²Open Targets, Wellcome Genome Campus, Hinxton, Cambridgeshire CB10 1SA, UK³Wellcome Sanger Institute, Wellcome Genome Campus, Hinxton, Cambridgeshire CB10 1SA, UK⁴Helsinki Institute of Life Science (HiLIFE), University of Helsinki, Haartmaninkatu 8, PO Box 63, Helsinki 00014, Finland⁵Faculty of Biological and Environmental Sciences, University of Helsinki, Viikinkaari 1, PO Box 65, Helsinki 00014, Finland⁶These authors contributed equally⁷Lead contact*Correspondence: pau.puigdevall@helsinki.fi (P.P.), helena.kilpinen@helsinki.fi (H.K.)<https://doi.org/10.1016/j.xgen.2023.100280>

SUMMARY

The use of induced pluripotent stem cells (iPSC) as models for development and human disease has enabled the study of otherwise inaccessible tissues. A remaining challenge in developing reliable models is our limited understanding of the factors driving irregular differentiation of iPSCs, particularly the impact of acquired somatic mutations. We leveraged data from a pooled dopaminergic neuron differentiation experiment of 238 iPSC lines profiled with single-cell RNA and whole-exome sequencing to study how somatic mutations affect differentiation outcomes. We found that deleterious somatic mutations in key developmental genes, notably the *BCOR* gene, are strongly associated with failure in dopaminergic neuron differentiation and a larger proliferation rate in culture. We further identified broad differences in cell type composition between incorrectly and successfully differentiating lines, as well as significant changes in gene expression contributing to the inhibition of neurogenesis. Our work calls for caution in interpreting differentiation-related phenotypes in disease-modeling experiments.

INTRODUCTION

Induced pluripotent stem cells (iPSC) are widely used to model human diseases, as they can differentiate to cell types and tissues that are otherwise not accessible. However, *in vitro* differentiation is subject to substantial technical and biological confounders that often lead to variable differentiation outcomes, a major challenge to scaling up and interpreting results from disease-modeling studies.¹ The underlying reasons for this variability are not well understood, but different factors have been proposed: protocol optimization,² culture maintenance,³ passage number,⁴ molecular determinants,⁵ inter-laboratory variation,⁶ cell line intrinsic properties,⁷ or the loss of iPSC heterogeneity in culture.⁸ Controlling differentiation variability of iPSCs is an essential step in achieving reliable disease models, in particular in the field of developmental biology where substantial efforts are under way to model the cell-level consequences of genetic findings in developmental and neuropsychiatric disorders.

The genetic background of an individual has been shown to account for 8%–23% of phenotypic variation in iPSCs.⁷ While this donor effect was driven primarily by common variants, rare variants and somatic mutations acquired either in the parental tissue (*in vivo*) or during the iPSC reprogramming process and culture maintenance (*in vitro*)⁹ are also likely to

contribute to the observed variation. For example, it has been shown that sub-clonal cancer-associated mutations in *P53* may provide growth advantage to stem cells in culture, given their increased frequency in embryonic stem cell lines.¹⁰ Also, the reprogramming of parental cells, such as skin-derived fibroblasts, can act as a bottleneck, leading to variants increasing or decreasing in frequency in the resulting population of iPSCs.¹¹ This can be particularly pronounced if the parental cells contain a higher-than-average number of mutations, as can be the case with skin-derived, UV-exposed cells. Although such acquired mutations might not cause a phenotype in iPSCs, they have the potential to affect specific differentiated cell types and lineages,¹² altering both their functionality and the overall cell type composition. Still, the contribution of somatic mutations to cellular differentiation has not been systematically explored.

In this study, we hypothesized that somatic mutations and rare germline variants in individual iPSC lines can affect their ability to differentiate. To test this hypothesis, we analyzed differentiation outcomes from four independent experiments that produced different target cell types from iPSC lines of the HipSci project⁷: dopaminergic neurons (DA),⁸ macrophages,¹³ sensory neurons,¹⁴ and definitive endoderm tissue¹⁵ (Figure 1A). We compared the exome-wide burden of acquired mutations and rare germline variants to the differentiation



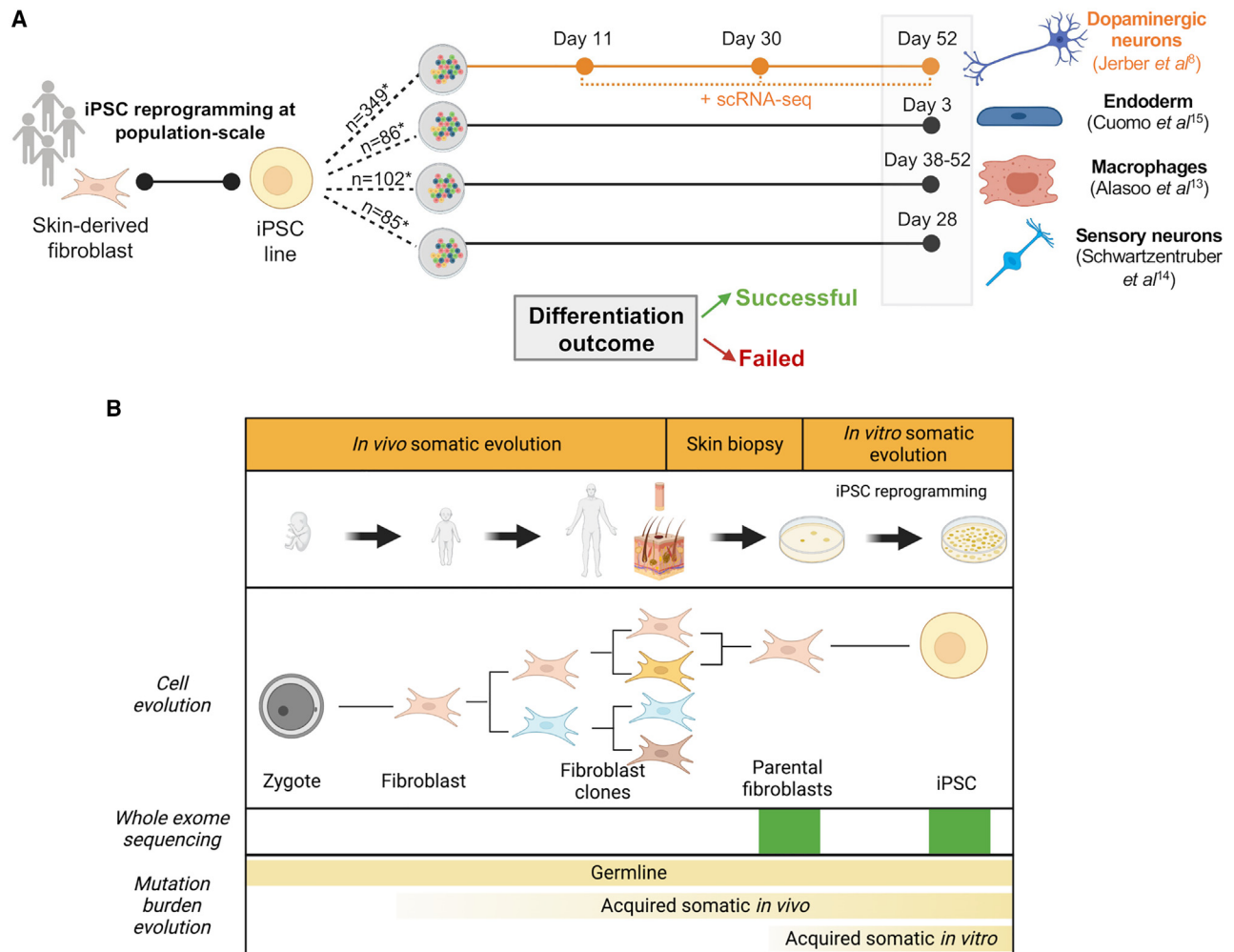


Figure 1. Study overview—cellular basis of variable differentiation outcomes in human iPSCs

(A) Human iPSC lines from the HipSci project were differentiated into macrophages, sensory neurons, endoderm tissue, and dopaminergic neurons, the latter being profiled with scRNA-seq in pools. iPSC lines were classified as having a failed or a successful differentiation outcome in each dataset. n, Number of iPSC lines per differentiation with available whole-exome sequencing (WES) also from the parental fibroblasts.

(B) We evaluated the genetic determinants of iPSC differentiation outcomes using WES data from 832 iPSC lines. For 384 of the 832 lines, WES data were also available for the parental fibroblasts, which allowed the identification of somatic mutations acquired *in vitro*.

outcomes of each line (Figure 1B), and used single-cell transcriptomes of the dopaminergic neurons⁸ to delineate in detail how deleterious variants influence the differentiation process of iPSC-derived neurons. We found that deleterious mutations in developmentally important genes can compromise the success of iPSC differentiation by increasing the growth rate of cell lines, leading to large differences in cell type composition, gene expression, and general outlier behavior of individual lines. Our work highlights somatic mutations as an important source of variation in iPSC-based models and calls for caution when interpreting differentiation-related phenotypes to understand disease. Our results support the notion that mutational processes that affect iPSCs and their differentiation to neurons reflect those that lead to somatic mosaicism during corticogenesis.

RESULTS

The exome-wide burden of acquired mutations does not explain the differentiation outcome

To test whether the overall burden of somatic mutations acquired by iPSC lines *in vitro* influenced their differentiation ability, we studied 384 cell lines (251 individual donors) from the HipSci project. Exomes were sequenced for both the parental fibroblast of donors and their derived iPSC lines, allowing us to distinguish between variants present already in the donors from those acquired, or positively selected for, in the subsequent reprogramming process (hereon “*in vitro*-acquired mutations”)¹¹ (STAR Methods). After excluding 17 hypermutated lines (>240 mutations), a median of 35 mutations (37 including copy number variants) was observed per exome in the iPSCs, of which 14 were

annotated as deleterious. The mutational burden was mainly donor-specific, as multiple lines from the same donor showed good correlation of mutation sites ($R^2 = 0.774$). In line with previous publications,¹⁶ half (50.5%) of the mutations (single nucleotide variants and dinucleotides) were predicted to be missense or loss-of-function (LoF). Also, 30% of the CNVs acquired by iPSCs overlapped with known CNVs annotated as pathogenic in ClinVar dbVar.¹⁷

We considered differentiation outcomes from four different tissues and cell types derived from the same cohort of HipSci donors: dopaminergic neurons⁸ (DA; $n = 126$ observed differentiations and $n = 349$ predicted differentiations, see STAR Methods, Table S1), sensory neurons¹⁴ ($n = 85$), macrophages¹³ ($n = 102$) and definitive endoderm¹⁵ ($n = 86$). For each of the cell types, we split the cell lines to those that differentiated successfully and to those that failed or had impaired capacity to give rise to the desired cell type (from hereon “successful” and “failed” lines) (STAR Methods). We then tested for association between the exome-wide mutational burden and the differentiation outcomes, and found no difference between successful and failed lines (all mutations, deleterious mutations (Figure 2A), and other variant classes (Figures S1A and S1B), $p_{\text{Adj}} > 0.05$). Similarly, no association was found between mutational burden and endoderm differentiation efficiency, which was defined as a continuous trait (Figure 2B). The identified somatic variants were located in longer genes than unmutated ones (t-test, $p = 1.02 \cdot 10^{-149}$) and were closer to repetitive elements (t-test, $p_{\text{Adj}} = 1.16 \cdot 10^{-23}$), as previously described for somatic variants acquired in postmitotic neurons (Figures S1C and S1D).^{18,19} The mutated genes showed reduced transcription ($p < 0.05$, t-test), but no differences in replication timing ($p = 0.49$, t-test, Roadmap Epigenomics Project) or promoter states ($p = 0.34$, chi-squared test, ENCODE BG02ES line) when compared with unmutated genes, in contrast to mutated genes in neurons (Figures S1E and S1F).^{20,21} Still, mutated genes in our study were enriched in published sets of somatic mutations originating early in brain development, mainly in the postzygotic stage²² ($p_{\text{Adj}} = 9.46 \cdot 10^{-4}$, hypergeometric test) or in the stem cell and neural progenitor stage¹⁸ ($p_{\text{Adj}} = 9.02 \cdot 10^{-5}$). This overlap indicates that mutational processes driving *in vivo* somatic mosaicism in human brain development may be partially mirrored by *in vitro* somatic mosaicism in iPSCs.

The burden of deleterious variants in *BCOR* is linked to differentiation failure in dopaminergic neurons

Mutations that impair the function of active genes in development might also have a critical role in altering cell line differentiation efficiency, even when they do not compromise cell survival in culture. We analyzed how burden differences in individual genes were linked to the differentiation outcome in the DA dataset. We focused on the total burden of deleterious mutations carried by each iPSC line, which includes somatic mutations acquired *in vitro* and *in vivo*, as well as germline variants (STAR Methods). We found that only one gene, *BCOR*, was significantly more mutated in failed lines compared with the successful lines (Wilcoxon rank-sum test, $p_{\text{Adj}} < 0.05$, $\log_2\text{FC} > 2.5$) (Figure 2C). This effect was consistently observed with all deleterious variants as well as LoF variants alone, and with both observed ($n = 183$ cell

lines, one line per donor; 48 failed, 135 successful) and predicted DA differentiation outcomes⁸ ($n = 793$ cell lines from 529 donors; 99 failed, 694 successful). Importantly, none of the lines that differentiated successfully in culture (i.e., with observed outcomes) carried an LoF mutation in the *BCOR* gene, while 22 of the 48 failed lines carried at least one (Figure S1G, Table S2). Beyond the binary outcome classification, we also observed the association between the deleterious mutational burden in *BCOR* with the continuous differentiation efficiency ($p_{\text{Adj}} = 1.06 \cdot 10^{-8}$, $n = 183$ lines), defined as the fraction of dopaminergic and serotonergic neurons at day 52, or with the predicted model scores⁸ ($p_{\text{Adj}} = 7.22 \cdot 10^{-57}$, $n = 793$ lines) (STAR Methods). We confirmed a significant reduction of *BCOR* expression between mutated (*BCOR* LoF) and unmutated lines across all time points ($p < 0.05$, Wilcoxon rank-sum test) (Figure S1H).

Although the mechanism for this association is unknown, the *BCOR* gene (a BCL6 repressor) is a known epigenetic regulator²³ that is both an oncogenic driver gene²⁴ and a developmental disorder-causing gene,²⁵ highlighting its key role in development. Previously, pathogenic mutations in the *BCOR* gene have been found to be recurrently mutated in blood-derived iPSC lines and positively selected for under iPSC culture conditions.¹¹ The gene is under strong mutational constraint, with only two predicted LoF SNVs (pLoF) observed in gnomAD²⁶ (version 2.1.1: 44.6 expected; LOEUF mutational constraint score 0.141). In addition, we did not find any *BCOR* LoF variants among the parental fibroblasts of the iPSC lines ($n = 253$), although they could still be present at very low frequencies as subclones. In our study, while the *BCOR* mutations driving impaired DA differentiation clearly increased in frequency during the reprogramming process, we cannot determine for certain whether they originated *in vivo* or *in vitro*.

A fraction of the lines that were classified as failed (26 of 48, differentiation efficiency < 0.2) do not carry any deleterious *BCOR* mutations, which likely indicates that other genes also contribute to DA differentiation failure but are not identified in our analysis due to limited sample size. To overcome this, we focused on the biological processes that control cellular differentiation and performed a gene ontology (GO) enrichment analysis on those genes that presented the largest mutational burden differences between failed and successful cell lines (top 10% and bottom 10% in fold change [FC], corresponding to 1,865 genes for each outcome, STAR Methods). We found that the genes mostly mutated in failed lines are involved in key neurodevelopmental functions, such as neuron fate commitment (GO:0048663, $p_{\text{Adj}} = 0.03$, OR = 1.99), response to axon injury (GO:0048678, $p_{\text{Adj}} = 0.015$, OR = 2.08) and midbrain development (GO:0030901, $p_{\text{Adj}} = 0.03$, OR = 1.8), consistent with the failed differentiation phenotype (Figure 2D, Table S3). Among the genes contributing to this enrichment in failed lines, we found examples of disease-associated genes²⁷: *CDC42* in intellectual disability,²⁸ *BMP4* in syndromic microphthalmia,²⁹ and *PMP22* in hereditary neuropathy.³⁰ On the contrary, mutations in successful lines disrupted genes involved in the positive regulation of neuron apoptotic process (GO:0043525, $p_{\text{Adj}} = 0.006$, OR = 2.59) and neuron fate specification (GO:0048665, $p_{\text{Adj}} = 0.001$, OR = 3.8), potentially contributing to a higher production of neurons throughout the differentiation.

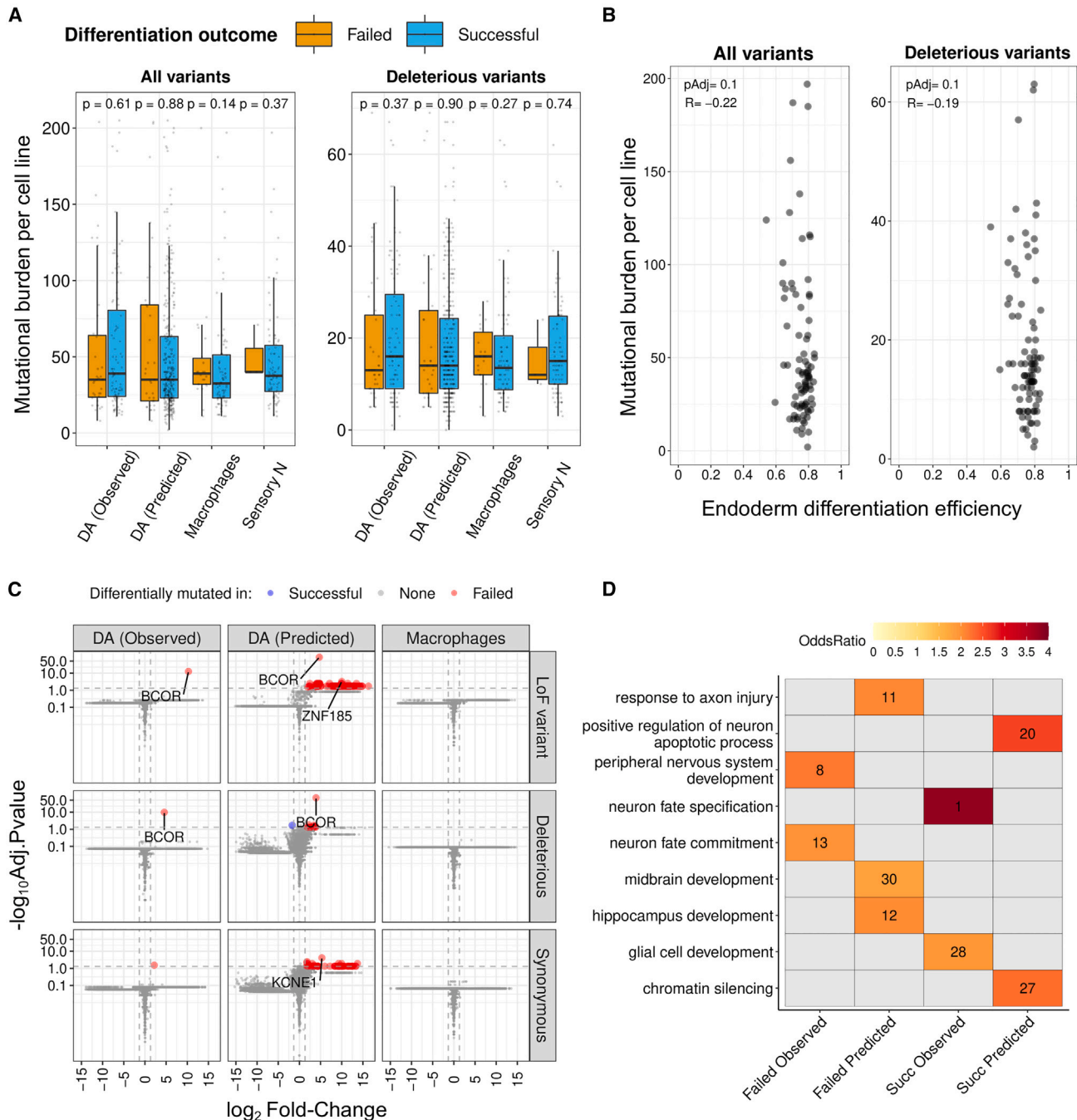


Figure 2. Effect of the mutational burden on iPSC differentiations

(A) Burden of somatic mutations in each cell line, either total (left) or deleterious (right), was not associated ($p > 0.05$, Wilcoxon rank-sum test) with the differentiation outcome in macrophages, sensory neurons, or dopaminergic neurons. Boxplot whiskers are within the 1.5 IQR value. See also [Figures S1A and S1B](#) and [Table S1](#).

(B) Burden of somatic mutations in each cell line, either total (left) or deleterious (right), was not associated with the differentiation efficiency in the endoderm ($p_{Adj} < 0.05$, Pearson correlation).

(C) Only the *BCOR* gene was consistently more mutated in failed lines than in successful lines from the dopaminergic differentiation, when considering damaging variation ($FC > 2.5$ (red), Wilcoxon rank-sum test, $p_{Adj} < 0.05$). See also [Figures S1G and S1H](#) and [Table S2](#).

(D) Gene ontology (GO) enrichment analysis revealed the impact of deleterious mutations on brain-related biological processes (hypergeometric test for GO term association, $p_{Adj} < 0.05$, red-colored tiles) contributing to either failed or successful DA differentiation in lines whose outcome was either observed or predicted. The number in each tile corresponds to the rank of the significant GO term, ordered by decreasing odds ratio within each analysis (only top-30 positions are illustrated). See also [Table S3](#).

Differentiation failure is driven by increased proliferation rate and *BCOR* LoF mutations

One of the unique features of the DA dataset is that the cell lines were differentiated as pools.⁸ When cell lines are cultured and differentiated together, individual lines may acquire mutations that give them growth advantage, such as those in cancer-associated genes, leading to an imbalanced representation of lines in the pool. In order to understand the potential mechanism by which the observed *BCOR* mutations impair DA differentiation, we studied the growth dynamics in the pooled DA dataset. We reanalyzed RNA-sequencing data from 846,841 single cells from 238 cell lines (230 donors) at three differentiation time points (days 11, 30, and 52, corresponding to progenitors, young neurons, and mature neurons, respectively) (STAR Methods, Figure S2), leading to a dataset consisting of 19 different pooled differentiations, including 7 to 24 cell lines per pool (Table S4).

We first evaluated how the proportion of cell lines sampled at the three time points ($n = 164$) changed over the course of DA differentiation, assuming initial equal amounts of each iPSC line (Figure 3A, STAR Methods). Specifically, we calculated an *in silico* proliferation rate for each line in a given pool by contrasting cell line proportions at specific time points to day 0. Although the Day52/Day0 proportion remained constant for most of the lines (mean = 1.0, 95% confidence interval 0.8–1.2) (Figure S3A), almost every pool contained at least one overrepresented line (up to 3–10x, depending on the pool), with a small fraction of lines being underrepresented (down to 7–700x). Interestingly, lines that failed to differentiate into neurons ($n = 50$) showed on average larger proliferation rates than successful lines ($n = 114$), with the difference being most significant at the last time point ($p = 2.8 \cdot 10^{-3}$, Wilcoxon rank-sum test) (Figure S3B). When we correlated this behavior with the mutational burden, we found that increased proliferation rates were driven by *BCOR* LoF mutations (Figure 3B). Specifically, failed lines with *BCOR* LoF mutations ($n = 20$) had a significantly higher proliferation rate than successful lines ($n = 114$) across the time points, a difference that was not observed with failed lines without *BCOR* LoF mutations ($n = 30$). Consistent with this, we found that the *BCOR* gene had the highest ratio (5:0) of annotated cancer driver mutations (LoF pathogenic Cosmic-Tier1 mutations) in failed lines compared with successful ones (STAR Methods). Taken together, these results suggest that proliferation advantage, caused by recurrent somatic mutations in key developmental genes like *BCOR*, has a negative effect on differentiation efficiency. Of note, when we compared cell line abundances in different types of replicate samples (Figure S3C), we found that the correlation of the fractions was substantially lower when replicates were differentiated as part of different pools ($R^2 = 0.136$, $n = 41$ lines) compared with replicates with the same pool background ($R^2 = 0.693$, $n = 31$ lines) (Figure 3C, STAR Methods). Still, pool replicates were mostly concordant in their differentiation outcome (33 of 36 lines). This suggests that other cell lines of a given pool can influence the growth dynamics of individual lines, likely due to the presence of non-cell-autonomous effects, but they are not sufficient to alter the differentiation outcome.

Poor differentiation outcomes manifest as shifts in cell type composition already at the progenitor stage

Next, we studied how early in the differentiation process cell type composition differences between failed ($n = 58$) and successful ($n = 163$) lines start to appear (STAR Methods). In order to better characterize cell type composition changes of cell lines across the three time points, we processed and clustered all cells in the DA dataset together (119 10x samples, Tables S5 and S6 and STAR Methods), contrary to the original study where time points were analyzed separately.⁸

We then used a negative binomial regression model to evaluate cell type composition changes between failed and successful lines (STAR Methods). The analysis revealed significant shifts in abundance for all major cell types (>2% fraction) as early as day 11, except for some floor-plate progenitors (FPP-1) and ependymal cells (Epend-1) (Figure 4A). Interestingly, cell lines that failed to generate mature neurons at day 52 showed an earlier commitment to either the dopaminergic (DA, $p\text{Adj} = 9.9 \cdot 10^{-47}$) or serotonergic (Sert-like, $p\text{Adj} = 6.1 \cdot 10^{-14}$) fate at day 11, with their neuroblasts clustering with young neurons, but failing to express the same neuronal markers. Similar evidence of accelerated neuronal maturation *in vivo* has been observed in an iPSC model of Kabuki syndrome caused by a heterozygous nonsense mutation in *KMT2D*,³¹ and in iPSC-derived brain organoids modeling schizophrenia.³² Also, different risk genes linked to autism spectrum disorders were recently shown to converge on an accelerated differentiation phenotype of GABAergic and deep-layer projection neurons.³³

At day 52, the overall lower fraction of neurons in failed lines was accompanied by a significantly larger proportion of astrocytes ($p\text{Adj} = 1.5 \cdot 10^{-36}$), ependymal-like cells ($p\text{Adj} = 7.7 \cdot 10^{-14}$), and of an unknown cell type (Unk-1, $p\text{Adj} = 1.1 \cdot 10^{-19}$). In agreement with these observations, iPSC lines with deleterious *BCOR* mutations also presented an altered cell type composition compared with lines without *BCOR* mutations, with a significant depletion of neuronal cell types (DA, $p\text{Adj} = 5.3 \cdot 10^{-6}$; Sert-like, $p\text{Adj} = 8.9 \cdot 10^{-8}$, Wilcoxon rank-sum test) accompanied by a significant excess of astrocytes ($p\text{Adj} = 1.3 \cdot 10^{-5}$), proliferative floor-plate progenitors (FPP-1, $p\text{Adj} = 1.9 \cdot 10^{-3}$), and one unknown cell type (Unk-1, $p\text{Adj} = 6.9 \cdot 10^{-3}$) (Figure S3D, STAR Methods). Importantly, we also found an association between the cell line proliferation rate and the abundance of those cell types, with faster-proliferating lines showing a depletion of DA neurons ($p\text{Adj} = 0.01$, Pearson correlation) and an excess of astrocytes ($p\text{Adj} = 0.004$) and proliferating progenitors (pro-FPP1, $p\text{Adj} = 0.004$) at day 52. (Figure 4B, STAR Methods). This suggests that differentiation failure is a consequence of a global, early shift in cell type composition caused by abnormally fast proliferation of cell lines that carry damaging mutations in key developmental genes such as *BCOR*.

Biological processes linked to failed differentiation manifest as differential gene expression

We tested whether differences in cell type composition between successful and failed lines also manifest as gene expression changes. For this, we performed a differential gene expression (DE) analysis between failed ($n = 58$) and successful ($n = 163$) cell lines within cell types and time points (STAR Methods). We

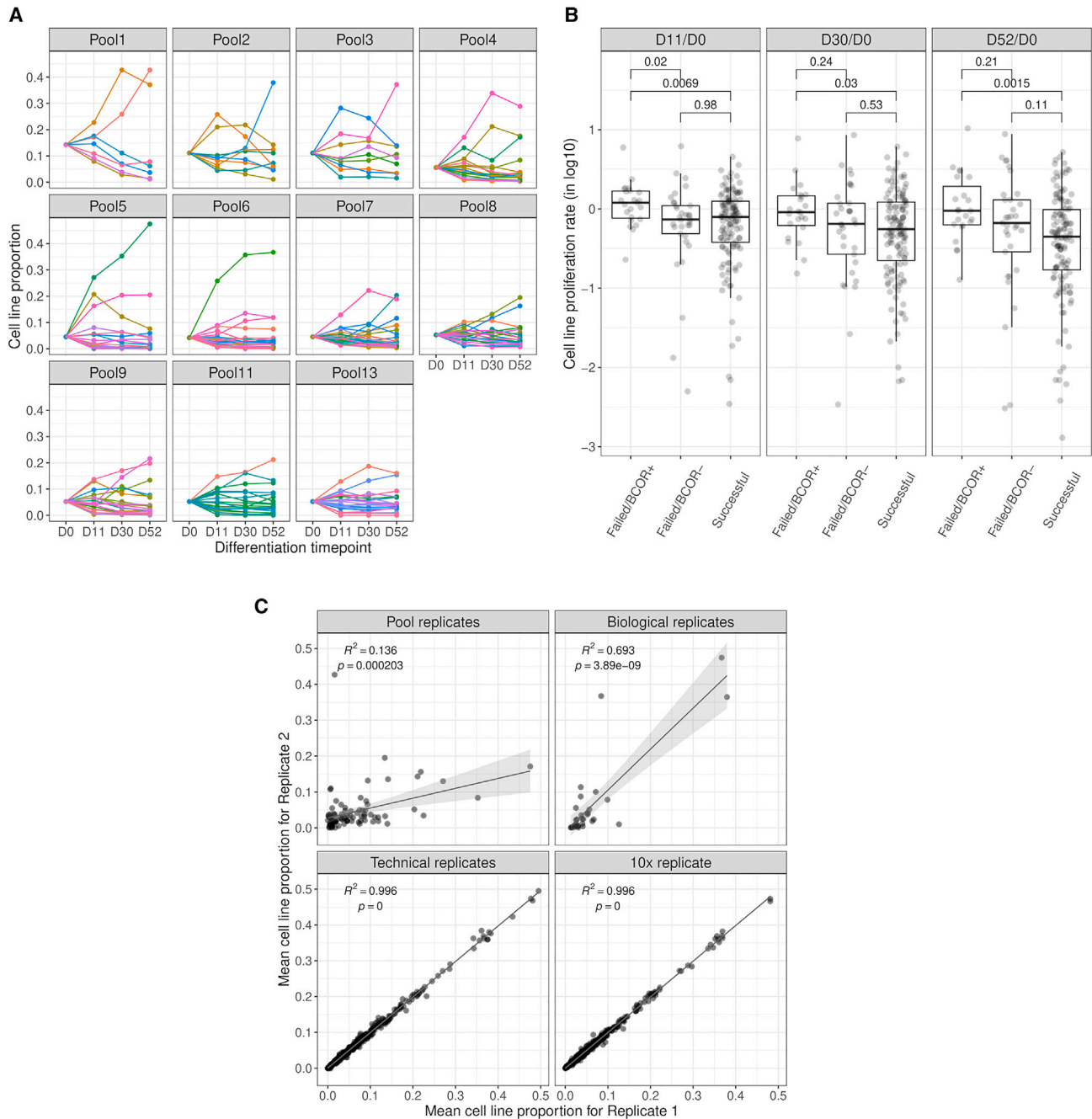


Figure 3. The proliferation rate of cell lines is influenced by the pool environment, but the highest rates were observed among failed lines with *BCOR* LoF mutations

(A) Cell line proportion throughout dopaminergic neuron differentiation (days 11, 30, and 52). We observed a consistent outlier behavior featured by 1–2 lines that proliferate significantly faster than other lines during pooled differentiation.

(B) Failed cell lines carrying at least one *BCOR* LoF mutation showed, on average, a higher proliferation rate than neurons that can differentiate successfully (D52/D0, $p = 0.0015$, Wilcoxon rank-sum test). Boxplot whiskers are within the 1.5 IQR value. See also Figures S3A and S3B.

(C) Cell line proportion could not be replicated between pool replicates, but it remained similar between biological replicates and showed minimal differences between technical and 10X replicates, as expected (linear regression, $p < 0.05$). The shaded area indicates 95% confidence interval on the proportion values. See also Figure S3C.

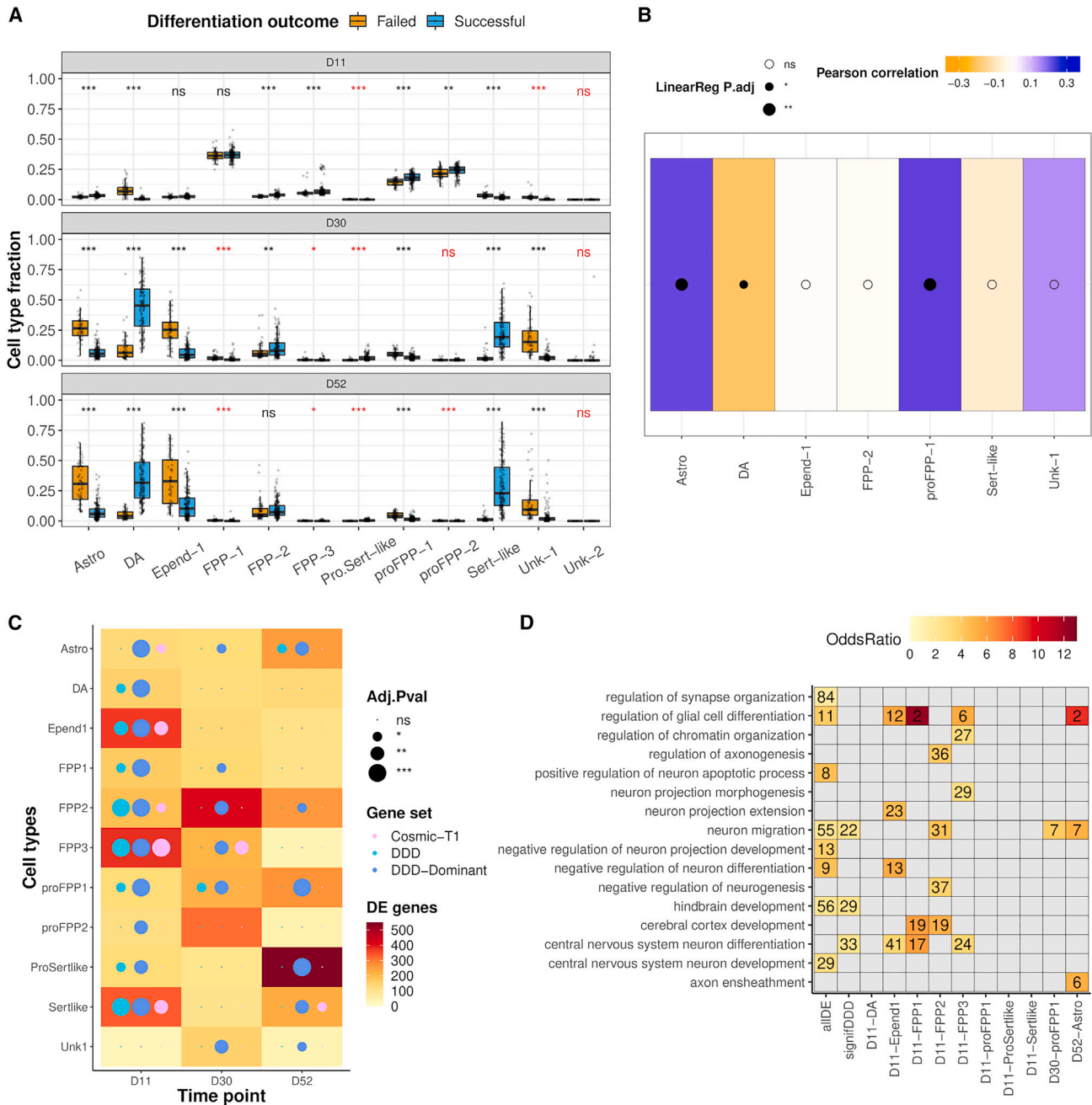


Figure 4. Failed and successful lines show major differences in cell type composition, gene expression, and functional enrichment

(A) Major cell types showed significant differences in composition as early as day 11 (negative binomial regression, STAR Methods), except for floor-plate progenitors type 1 (FPP-1) and ependymal-like cells (Epend-1). Neuroblasts from failed lines showed an earlier commitment to dopaminergic (DA) or serotonergic-like (Sert-like) fate. Minor cell types (<2% abundance) are shown in red. Boxplot whiskers are within the 1.5 IQR value. See STAR Methods for cell type abbreviations.

(B) High proliferation rates were associated with significant changes on cell type composition at day 52 linked to a depletion (in orange) of dopaminergic (DA, $p < 0.05$ (*), linear regression) neurons and an excess (in blue) of astrocytes (Astro) and proliferative floor-plate progenitors type 1 (proFPP-1, $**p < 0.01$). See STAR Methods for cell type abbreviations.

(C) Most of the differentially expressed genes at day 11 are enriched in developmental disorder genes (DDD, cyan), especially when considering those that act in a dominant fashion (DDD-dominant, blue) (chi-squared test, STAR Methods). Also, some of the cell types show an enrichment in cancer-associated genes (Cosmic Tier 1, magenta). See also Figures S4A and S4B.

The significance level in (A–C) was indicated as follows: $pAdj > 0.05$ (ns), $pAdj < 0.05$ (*), $pAdj < 0.01$ (**), $pAdj < 0.001$ (***).

(legend continued on next page)

identified between 50 and 500 DE genes per test, which, importantly, were not correlated with the number of cells observed per outcome (Figure S4A). While the number of DE genes was relatively constant throughout differentiation in certain lineages (dopaminergic, astrocytes, floor-plate progenitors type 1), others showed time-point-specific differences. Remarkably, in most of the cell types at the progenitor stage, gene sets known to cause developmental disorders³⁴ (DDD) were overrepresented among the DE list ($\text{adj.}p < 0.05$, chi-squared test), in particular when only dominant DDD genes were considered. Likewise, cancer-associated genes³⁵ (Cosmic-Tier1) known to influence cellular proliferation were overrepresented in five cell types at day 11, one at day 30, and another at day 52 (Figure 4C).

We then performed a GO enrichment analysis (STAR Methods) on the 10 cell types with a significant proportion of differentially expressed DDD genes. We found several biological processes related to neurodevelopment among the top-25 enriched terms ($\text{adj.}p < 0.05$, ordered by odds ratio) (Figure 4D, Table S7), including the regulation of glial cell differentiation (GO:0045685, day 11) and cerebral cortex development in progenitors (GO:0021987, day 11), as well as the neuron projection extension in ependymal-like cells (GO:1990138, day 11). When aggregating all the detected DE genes in the analysis (any cell type), we found processes strongly linked to failed differentiation, such as the positive regulation of neuron apoptotic process (GO:0043525) and the negative regulation of neuron differentiation (GO:0045665). We also analyzed the changes in pathway regulation on the seven cell types with an excess of cancer-associated DE genes (STAR Methods, Figure S4B), and consistently identified hallmarks of cellular proliferation: upregulation of the tumor suppressor P53, activation of MYC targets, and exacerbated oxidative phosphorylation. This functional enrichment of DE genes is consistent with that of mutated genes in failed lines (Figure 2D).

Proliferation rate predicts cell type outlier status of cell lines

Cellular differentiation is a dynamic process with global changes in the composition of cell populations over time. Although differentiation success is usually defined by the final yield of the desired cell type, this can give an incomplete picture of the variability in the differentiation process. To characterize such variability, we analyzed all cell lines with reliable cell fraction estimates (day 11, $n = 172$; day 30, $n = 187$; day 52, $n = 209$, STAR Methods) to identify those that were outliers in terms of their cell type composition. For this purpose, we computed a Z score per line for each cell type and time point combination and assigned as outliers those cell lines with $|Z \text{ score}| > 2$ (Figure 5A, STAR Methods). Under this classification, we identified 156 cell lines (175 considering pool replicates as independent lines) that were an outlier in at least one of the time points (day 11, $n = 55$; day 30, $n = 78$; day 52, $n = 104$), most of which had abnormally large cell type fractions. Only on day 11, 16 cell lines showed abnormally low fractions of progenitors and astrocytes,

which were compensated by abnormally large fractions of other cell types. We also observed an overall increase in cell type fraction variability at later stages of differentiation.

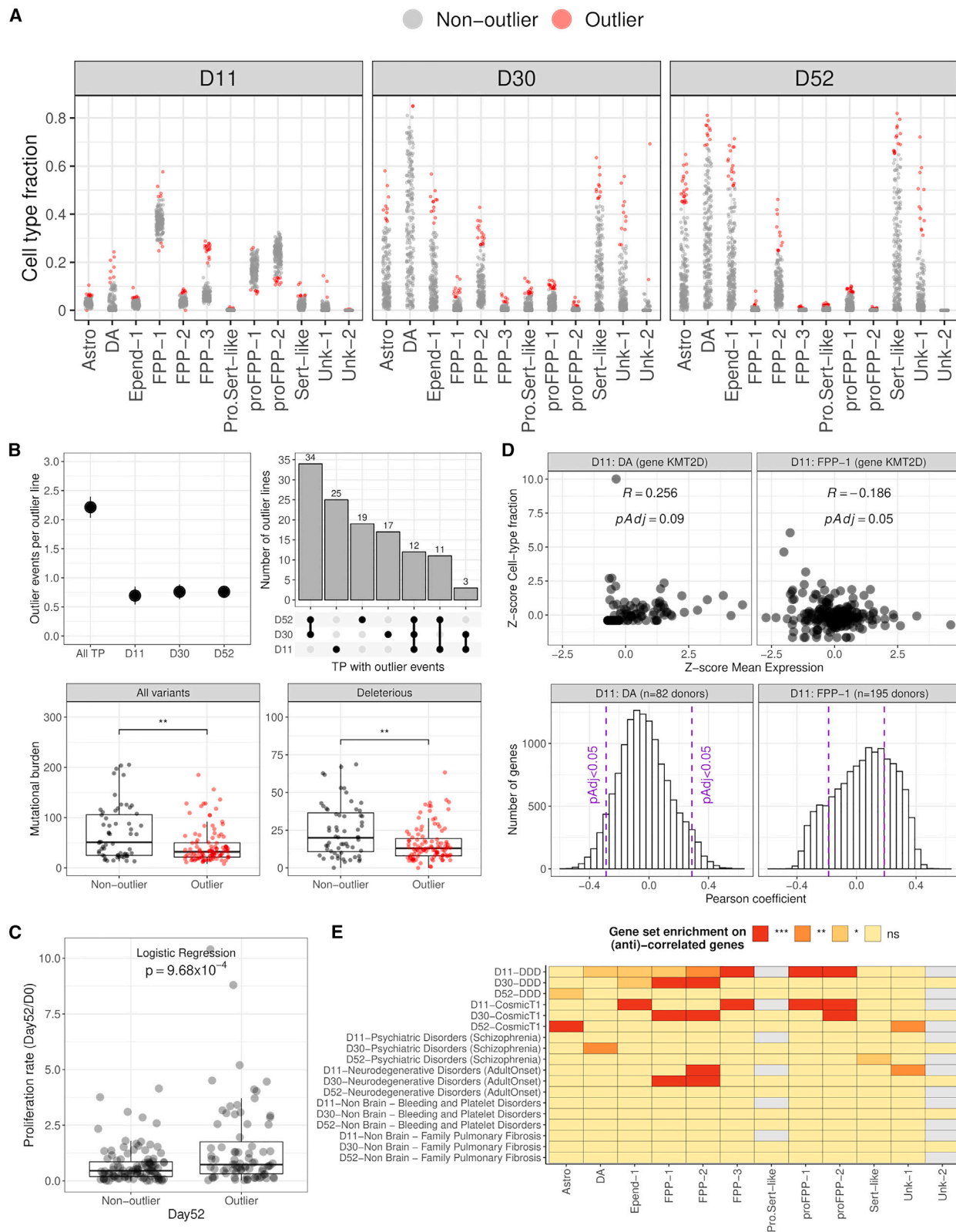
To further characterize the outlier behavior, we calculated the number of times an outlier line shows an abnormal cell type fraction across the differentiation (outlier event, STAR Methods). On average, we observed 2.21 outlier events per line (2.03–2.39, 95% CI) with even contributions per time point (Figure 5B, upper). When focusing only on the cell lines profiled at the three time points ($n = 112$ lines), we observed that they tend to show outlier events most frequently at the two consecutive latest time points (day 30 and day 52) or just initially (day 11), likely due to the final plating of neurons occurring between the first and later time points. Only 12 cell lines showed outlier behavior in all time points. Unexpectedly, when we explored the correlation of somatic mutational burden acquired *in vitro* with outlier behavior ($n = 148$ lines), we observed a significant reduction of burden ($p < 0.01$, Wilcoxon rank-sum test) in the outlier group (Figure 5B, lower). This difference was observed for both total and deleterious mutations, but when detaching the outlier status per time point, the difference remained significant only at day 30 (Figure S5A, STAR Methods).

Although observing uneven cell type fractions is common among wild-type iPSC lines in pooled experiments, we found that larger proliferation rates at day 52 were associated with the outlier behavior ($p = 9.68 \cdot 10^{-4}$, logistic regression, $n = 159$ lines) (Figure 5C). To identify which genes might be driving this behavior, we correlated cell-type-specific gene expression with changes in cell type composition (Figure 5D, STAR Methods). Among the significant associations, including positively and negatively correlated genes, we observed a strong enrichment of DDD genes ($p.\text{Adj} < 0.001$, hypergeometric test) in most of the cell types at the progenitor stage (Figure 5E, STAR Methods), including *BCOR* (Figure S5B). Similarly, we observed that seven of the nine cell type associations enriched in cancer-associated genes were also enriched among DDD genes, as expected from the significant overlap between the two gene sets ($p < 2.2 \cdot 10^{-16}$, chi-squared test). A more limited enrichment in adult-onset neurodegenerative disorder genes³⁶ was also observed for floor-plate progenitors (FPP). However, for schizophrenia genes,³⁷ weaker but still significant associations were observed only for dopaminergic (day 30) and serotonergic neurons (day 52). As expected, no enrichment was observed in gene panels for non-brain disorders.³⁶ Overall, this suggests that the regulation of developmental genes during early neural induction is critical for determining progenitor abundance, and as shown for the *BCOR* gene, for influencing proliferation rate and differentiation success *in vitro*.

DISCUSSION

One of the biggest limitations of iPSC-based disease modeling is our poor understanding, and control, of factors that influence the

(D) Functional enrichment of biological processes among differentially expressed (DE) genes from all (*allDE*), several (*signifDDD*), or unique cell types (hypergeometric test for GO term association, $p.\text{Adj} < 0.05$ and $\text{FC} > 1.5$). Overrepresented processes in failed lines include neuron development and neuron maturation as previously observed with genes showing differential deleterious burden between failed and successful lines. The number in each tile corresponds to the ranked position of the significant GO term, ordered by decreasing odds ratio within each analysis. See also Table S7.



(legend on next page)

capacity of cell lines to differentiate successfully and reproducibly. Recently, it was proposed that the large variability associated with differentiation is primarily explained by cell-intrinsic factors,⁸ rather than experimental or other technical factors. Genetic variation has previously been shown to drive molecular heterogeneity in iPSCs^{7,38–40} and in hESC,⁴¹ but large-scale studies looking at the role of genetic variation in differentiation are only beginning to emerge. In particular, somatic mutations acquired prior to the differentiation, either *in vivo* during parental tissue clonal evolution or *in vitro* during iPSC reprogramming and culture maintenance, are potential contributors to variation in differentiation efficiency. Interpreting such variation correctly is critical for developing better models of development and diseases, particularly in the field of neurodevelopment, where disease-modeling efforts are currently rapidly increasing, due to advances in identifying the genetic underpinnings of psychiatric and developmental disorders.^{42,43}

Here, we present an attempt to link differentiation outcomes to somatic mutations in human iPSC lines from the HipSci resource, which offers a unique opportunity to study multiple cell types independently derived from the same iPSC lines. Further, with exome sequencing available for both iPSCs and their parental fibroblasts, we were able to focus also on the subset of damaging mutations acquired *in vitro*, which are particularly relevant for abnormal differentiation outcomes.

One of the key insights from our work is that although the total burden of acquired mutations in iPSC lines is not predictive of their differentiation outcome, deleterious mutations in the core genes of a given differentiation system can cause unwanted effects on differentiation. This effect is likely not limited to mutations acquired *in vitro*, as mutations and rare variants in the genetic background of the parental cells selected for reprogramming may account for a considerable fraction of differentiation variability, even if not affecting reprogramming directly. In support of this, we found that somatic deleterious mutations in the *BCOR* gene are strongly associated with differentiation failure in human dopaminergic neurons. The effect was seen with 183 observed differentiations as well as 793 predicted differentiation outcomes of iPSC to dopaminergic neurons.⁸ The sensitivity to *BCOR* deleterious mutations is supported by the strong selection against predicted LoF variants in the Genome Aggregation Database.⁴⁴ Further, a high prevalence of acquired *BCOR* muta-

tions was previously found in blood-derived iPSC lines, and it was shown that they likely arose after reprogramming through positive selection for *BCOR* dysfunction.¹¹ In our dataset, damaging *BCOR* variants were only observed in the iPSC lines, although they could have originated *in vivo* and be present in parental fibroblasts as subclones at very low frequencies that later underwent positive selection *in vitro*.

BCOR is a key transcriptional regulator during embryogenesis. It is part of a specific type of polycomb repressive complex that mediates transcriptional repression through epigenetic modifications of histones²⁴ and has been shown to have a key role in regulating the pluripotent state and differentiation. Like many other chromatin-related genes, *BCOR* is annotated both as a developmental disorder gene and a cancer driver gene.^{35,45,46} In line with this dual role, we observed that failed lines with deleterious *BCOR* mutations showed significantly larger proliferation rates than lines that differentiated successfully, suggesting that monitoring cell line proliferation rates prior to differentiation may be an effective way to screen out lines that will not differentiate correctly.⁴⁷ Further, abnormal proliferation has been reported as a phenotype in multiple iPSC-based disease models, such as Kabuki syndrome³¹ or in tuberous sclerosis, where an hyperproliferative population of interneuron progenitors in brain organoids was identified as the underlying cause for the distinctive phenotype of brain tumors and cortical malformations.⁴⁸

Although the *BCOR* gene was not part of the expression signature of failed differentiation in specific iPSC populations ($n = 184$ lines),⁸ we observed that *BCOR* expression in dopaminergic neurons was negatively associated with final neuron abundance, and was also linked to the abundance of progenitor populations earlier in the differentiation. As an epigenetic modulator of stemness and differentiation, it remains unknown whether the expressivity of *BCOR* LoF mutations manifests already in iPSCs, at precursor stage or at both, diverting neuron differentiation toward astrocytes and ependymal-like cells.

Despite the strong association of *BCOR* mutations with differentiation failure, not all of the failed lines carried damaging variants in that gene, suggesting that other genes are involved as well. Therefore, we also analyzed the most differentially mutated genes in each differentiation outcome to pinpoint the biological processes that were disrupted by deleterious mutations. Interestingly, genes that were mutated mostly in failed lines were

Figure 5. Cell lines in the pooled differentiation displayed common outlier behavior in cell type composition

(A) Most of the outlier cell lines showed an excess of a particular cell type throughout the differentiation, except for some lines with a reduced population of astrocytes and progenitors at day 11.

(B) Upper: On average, each outlier line showed 2.21 outlier events per differentiation, but less than 1 event per time point (bars, 95% CI). Also, most of the lines displayed the outlier behavior either simultaneously at days 30 and 52 (young and mature stage), or just at day 11 (progenitor stage); lower: Lines with at least one abnormal cell type abundance throughout the differentiation (outlier event) showed a significant reduction in the somatic burden of acquired mutation *in vitro* than non-outliers (total burden, $p = 3.6 \cdot 10^{-3}$; deleterious, $p = 2.7 \cdot 10^{-3}$; Wilcoxon rank-sum test). Boxplot whiskers are within the 1.5 IQR value. See also Figure S5A. (C) The mean proliferation rate per line (day 52/day 0) was higher in outlier lines than in non-outlier lines ($p = 9.68 \cdot 10^{-4}$, logistic regression). Boxplot whiskers are within the 1.5 IQR value.

(D) Upper: Z score correlation of gene expression (i.e., *KMT2D*) and cell type proportions of floor-plate progenitors type 1 (FPP-1) and neuroblasts committing to dopaminergic neurons (DA) at day 11. Each dot is an iPSC line; lower: The distribution of Pearson correlation coefficients for all genes expressed in previous cell types at day 11. See also Figure S5B.

(E) The abundance of progenitor populations was associated with the expression of genes in developmental disorder (DD) and cancer-associated (Cosmic-Tier1) genes, and to a lesser extent in adult-onset neurodegenerative disorder genes. In schizophrenia, the association is only observed with genes expressed in neurons and no enrichment is observed for non-brain disorders (hypergeometric test for overrepresentation, Benjamini-Hochberg multiple-test correction). Significance levels: pAdj >0.05 (ns, yellow), pAdj <0.05 (*, golden yellow), pAdj <0.01 (**, orange), pAdj <0.001 (***, red).

enriched in neurodevelopmental processes linked to neuron fate commitment, response to axon injury, or midbrain development. In successful lines, we observed an enrichment of brain-related processes that are likely to boost neuron production by disrupting the positive regulation of neuron apoptotic processes. While our study is limited to identifying acquired mutations only during iPSC reprogramming, it is possible that somatic mosaicism in neurons also plays a role in determining the final differentiation outcome. To this end, mutated genes from our study significantly overlapped with published lists of somatic mutations that originated during early cortical development,^{18,22} highlighting that mutation-selection processes driving *in vitro* somatic mosaicism could mirror those observed *in vivo* during brain formation. If confirmed, this would have major implications for disease modeling, as somatic mosaicism observed *in vitro* could be used to understand the clinical impact of this process *in vivo*. Future efforts in profiling exomes of iPSC-derived neurons will provide further insights on the role of somatic mutations in differentiation systems and on new potential applications for developmental studies.

To better characterize the cell type composition dynamics throughout the DA differentiation process, we introduced a critical modification to the analysis in the original study.⁸ Specifically, we clustered all cells at once, rather than per time point. While we lose some granularity in the definition of cell types, this approach allowed us to observe cell type composition changes per line across cellular lineages, tracing the commitment of neuroblasts to young and mature neurons. We identified a larger fraction of neuroblasts committing to dopaminergic and serotonergic neurons in failed lines, suggesting an accelerated maturation of progenitors potentially linked to the proliferative phenotype. In this scenario, failed lines could progress faster to differentiation initiation after neural induction, promoting an early production of neuroblasts with defects in neuronal commitment.

Finally, we compared the extent of DE in each cell type across time points and conditions between failed and successful lines. With these comparisons, we sought to identify the key regulator genes across the different stages of neurodevelopment and across different biological processes. Many cell types at the progenitor stage (day 11) showed an enrichment of DE genes corresponding to key developmental genes, either DDD or cancer-associated. In those cell types, the differentially regulated neurodevelopmental processes clearly overlap with those affected by deleterious mutations in failed lines. We hypothesize that among the DE genes, there is a potential list of new developmental disorder (DD) candidates, whose clinical significance should be evaluated.

Any differentiation process involves a dynamic evolution of cell types, which does not necessarily fit into a failed or successful outcome based on an arbitrary threshold. To avoid overlooking other relevant changes, we analyzed general behavior in cell type composition. We found that 64.3% of lines in pooled experiments occasionally display abnormal cell type fractions during the differentiation process. This outlier behavior reflects the large variability in cell type composition during *in vitro* pooled differentiations, likely resulting from the combination of donor effects, non-cell-autonomous effects between lines and stochasticity. Although such effects are indeed a limitation of the pooled study

design that can affect cell line abundance, they rarely compromise the ultimate differentiation outcome in our dataset. Also, the periodicity of outlier events suggests that they tend to happen either consecutively in the last two time points or only at the first one, which can be explained by the experimental design, as cells were only passaged at day 20. Even more importantly, we found that outlier behavior was strongly associated with larger proliferation rates in cell lines, possibly implying that acquired mutations in other genes that also increase proliferation activity could be behind the abnormal cell type composition. However, since the mutational recurrence in all other genes was substantially lower than in *BCOR*, this study was not sufficiently powered to detect population-level evidence for this possibility. Finally, we did not observe a higher burden of acquired mutations in outlier lines when compared to non-outlier lines, but rather the opposite. These observations suggest that while individual deleterious mutations can define differentiation outcomes, the determinants of outlier behavior during neuronal differentiation are likely more varied.

In summary, our study demonstrates that although iPSC models are an excellent tool for studying neurodevelopment and developmental disorders, results from differentiated cell types should be interpreted with caution. We studied a large number of iPSC lines derived from healthy individuals and observed that deleterious mutations in genes known to cause developmental disorders cause differentiation defects via transcriptional and cell type composition changes during neuronal differentiation. Our work highlights somatic mutations as a significant source of variation in iPSC-based disease models and further emphasizes the importance of comprehensively assaying the genomes of iPSC lines prior to their experimental use to achieve reproducible research.

Limitations of the study

This study considers only mutations that originated or were positively selected during iPSC reprogramming from parental fibroblasts, or that were present at iPSC culture. Consequently, we lack mutational information from differentiated cell types, i.e., somatic mutations that may have occurred during the differentiation process and might also contribute to variable differentiation outcomes. As for the DA dataset, the pooling strategy reduces the unwanted batch effect between lines, but introduces non-cell-autonomous effects that might alter the growth dynamics of individual lines. Finally, we did not functionally validate the impact of *BCOR* LoF mutations on differentiation failure and the gene expression reduction that we observed with single-cell transcriptomics data.

STAR★METHODS

Detailed methods are provided in the online version of this paper and include the following:

- [KEY RESOURCES TABLE](#)
- [RESOURCE AVAILABILITY](#)
 - Lead contact
 - Materials availability
 - Data and code availability

METHOD DETAILS

- Somatic mutations acquired *in vitro* (SMAV)
- Functional annotation of SMAV
- Differentiation outcome of iPSC-derived cell types
- Gene burden differences upon differentiation outcome
- GO enrichment analysis (mutational burden)
- Reanalysis of pooled single-cell data (DA)
- Pool reproducibility of cell line abundance
- Cell line proliferation in DA differentiation
- Annotation of cancer-driver mutations
- Differential abundance analysis
- Impact of deleterious burden in *BCOR*
- DE analysis between failed and successful lines
- GO enrichment analysis (gene expression)
- Gene set enrichment analysis (cancer genes)
- Outlier lines in cell type composition
- Gene expression and cell type abundance links

SUPPLEMENTAL INFORMATION

Supplemental information can be found online at <https://doi.org/10.1016/j.xgen.2023.100280>.

ACKNOWLEDGMENTS

This work was funded by the UK Medical Research Council (MR/L016311/1; MRC eMedLab Medical Bioinformatics career development award to H.K.), Helsinki Institute of Life Science (H.K.), the ICH CIO (S.C. and P.P.) and the NIHR GOSH BRC (S.C., P.P., and H.K.). The views expressed are those of the author(s) and not necessarily those of the NHS, the NIHR, or the Department of Health. The authors acknowledge Zenodo, the data repository developed under the European Open Science Infrastructure (OpenAIRE) to facilitate the open access to our metadata and normalized gene count matrices. The authors gratefully acknowledge Drs. Daniel Gaffney, Oliver Stegle, and Florian Merkle for early access to the dopaminergic neuron single-cell dataset, and Drs. Daniel Seaton and Anna Cuomo for assistance with the DA data. The authors also acknowledge Drs. Matthew Hurles, Sebastian Gerety, and Osama Arshad for their feedback on the project. Illustration in Figures 1 and S4C and the graphical abstract were created with BioRender.com.

AUTHOR CONTRIBUTIONS

The main analysis (single-cell data processing, data preparation, and data analysis) was performed by P.P. under the supervision of S.C. and H.K. J.J. performed the cell type annotation and provided guidance with the data preparation. P.D. produced the mutation callset for the somatic acquired variation. P.P., H.K., and S.C. wrote and edited the manuscript. P.P. and H.K. conceived the study.

DECLARATION OF INTERESTS

The authors declare no competing interests.

INCLUSION AND DIVERSITY

We support inclusive, diverse, and equitable conduct of research.

Received: June 11, 2022

Revised: November 11, 2022

Accepted: February 23, 2023

Published: March 23, 2023

REFERENCES

1. Rowe, R.G., and Daley, G.Q. (2019). Induced pluripotent stem cells in disease modelling and drug discovery. *Nat. Rev. Genet.* **20**, 377–388.
2. Flippe, L., Gaignerie, A., Sérazin, C., Baron, O., Saulquin, X., Themeli, M., Guillonnet, C., and David, L. (2020). Rapid and reproducible differentiation of hematopoietic and T cell progenitors from pluripotent stem cells. *Front. Cell Dev. Biol.* **8**, 577464.
3. Chen, K.G., Mallon, B.S., McKay, R.D.G., and Robey, P.G. (2014). Human pluripotent stem cell culture: considerations for maintenance, expansion, and therapeutics. *Cell Stem Cell* **14**, 13–26.
4. Koehler, K.R., Tropel, P., Theille, J.W., Kondo, T., Cummins, T.R., Viville, S., and Hashino, E. (2011). Extended passaging increases the efficiency of neural differentiation from induced pluripotent stem cells. *BMC Neurosci.* **12**, 82.
5. Cacchiarelli, D., Qiu, X., Srivatsan, S., Manfredi, A., Ziller, M., Overbey, E., Grimaldi, A., Grimsby, J., Pokharel, P., Livak, K.J., et al. (2018). Aligning single-cell developmental and reprogramming trajectories identifies molecular determinants of myogenic reprogramming outcome. *Cell Syst.* **7**, 258–268.e3. <https://doi.org/10.1016/j.cels.2018.07.006>.
6. Volpato, V., Smith, J., Sandor, C., Ried, J.S., Baud, A., Handel, A., Newey, S.E., Wessely, F., Attar, M., Whiteley, E., et al. (2018). Reproducibility of molecular phenotypes after long-term differentiation to human iPSC-derived neurons: a multi-site omics study. *Stem Cell Rep.* **11**, 897–911.
7. Kilpinen, H., Goncalves, A., Leha, A., Afzal, V., Alasoo, K., Ashford, S., Bala, S., Bensaddek, D., Casale, F.P., Culley, O.J., et al. (2017). Common genetic variation drives molecular heterogeneity in human iPSCs. *Nature* **546**, 370–375.
8. Jerber, J., Seaton, D.D., Cuomo, A.S.E., Kumasaka, N., Haldane, J., Steer, J., Patel, M., Pearce, D., Andersson, M., Bonder, M.J., et al. (2021). Population-scale single-cell RNA-seq profiling across dopaminergic neuron differentiation. *Nat. Genet.* **53**, 304–312.
9. D'Antonio, M., Benaglio, P., Jakubosky, D., Greenwald, W.W., Matsui, H., Donovan, M.K.R., Li, H., Smith, E.N., D'Antonio-Chronowska, A., and Frazer, K.A. (2018). Insights into the mutational burden of human induced pluripotent stem cells from an integrative multi-omics approach. *Cell Rep.* **24**, 883–894.
10. Merkle, F.T., Ghosh, S., Kamitaki, N., Mitchell, J., Avior, Y., Mello, C., Kashin, S., Mekhoubad, S., Ilic, D., Charlton, M., et al. (2017). Human pluripotent stem cells recurrently acquire and expand dominant negative P53 mutations. *Nature* **545**, 229–233.
11. Rouhani, F.J., Zou, X., Danecek, P., Badja, C., Amarante, T.D., Koh, G., Wu, Q., Memari, Y., Durbin, R., Martincorena, I., et al. (2022). Substantial somatic genomic variation and selection for BCOR mutations in human induced pluripotent stem cells. *Nat. Genet.* **54**, 1406–1416.
12. Volpato, V., and Webber, C. (2020). Addressing variability in iPSC-derived models of human disease: guidelines to promote reproducibility. *Dis. Model. Mech.* **13**, dmm042317. <https://doi.org/10.1242/dmm.042317>.
13. Alasoo, K., Rodrigues, J., Mukhopadhyay, S., Knights, A.J., Mann, A.L., Kundu, K., HIPSCI Consortium; Hale, C., Dougan, G., and Gaffney, D.J. (2018). Shared genetic effects on chromatin and gene expression indicate a role for enhancer priming in immune response. *Nat. Genet.* **50**, 424–431.
14. Schwartzentruber, J., Foskolou, S., Kilpinen, H., Rodrigues, J., Alasoo, K., Knights, A.J., Patel, M., Goncalves, A., Ferreira, R., Benn, C.L., et al. (2018). Molecular and functional variation in iPSC-derived sensory neurons. *Nat. Genet.* **50**, 54–61.
15. Cuomo, A.S.E., Seaton, D.D., McCarthy, D.J., Martinez, I., Bonder, M.J., Garcia-Bernardo, J., Amatya, S., Madrigal, P., Isaacson, A., Buettner, F., et al. (2020). Single-cell RNA-sequencing of differentiating iPSC cells reveals dynamic genetic effects on gene expression. *Nat. Commun.* **11**, 810.
16. Yizhak, K., Aguet, F., Kim, J., Hess, J.M., Kübler, K., Grimsby, J., Frazer, R., Zhang, H., Haradhvala, N.J., Rosebrock, D., et al. (2019). RNA sequence analysis reveals macroscopic somatic clonal expansion across

- normal tissues. *Science* 364, eaaw0726. <https://doi.org/10.1126/science.aaw0726>.
17. Landrum, M.J., Lee, J.M., Benson, M., Brown, G.R., Chao, C., Chitipiralla, S., Gu, B., Hart, J., Hoffman, D., Jang, W., et al. (2018). ClinVar: improving access to variant interpretations and supporting evidence. *Nucleic Acids Res.* 46, D1062–D1067.
 18. Wei, P.-C., Chang, A.N., Kao, J., Du, Z., Meyers, R.M., Alt, F.W., and Schwer, B. (2016). Long neural genes harbor recurrent DNA break clusters in neural stem/progenitor cells. *Cell* 164, 644–655.
 19. Coufal, N.G., Garcia-Perez, J.L., Peng, G.E., Yeo, G.W., Mu, Y., Lovci, M.T., Morell, M., O’Shea, K.S., Moran, J.V., and Gage, F.H. (2009). L1 retrotransposition in human neural progenitor cells. *Nature* 460, 1127–1131.
 20. Lodato, M.A., Woodworth, M.B., Lee, S., Evrony, G.D., Mehta, B.K., Karger, A., Lee, S., Chittenden, T.W., D’Gama, A.M., Cai, X., et al. (2015). Somatic mutation in single human neurons tracks developmental and transcriptional history. *Science* 350, 94–98.
 21. Reid, D.A., Reed, P.J., Schlachetzki, J.C.M., Nitulescu, I.I., Chou, G., Tsui, E.C., Jones, J.R., Chandran, S., Lu, A.T., McClain, C.A., et al. (2021). Incorporation of a nucleoside analog maps genome repair sites in postmitotic human neurons. *Science* 372, 91–94.
 22. Rodin, R.E., Dou, Y., Kwon, M., Sherman, M.A., D’Gama, A.M., Doan, R.N., Rento, L.M., Girsakis, K.M., Bohrsen, C.L., Kim, S.N., et al. (2021). The landscape of somatic mutation in cerebral cortex of autistic and neurotypical individuals revealed by ultra-deep whole-genome sequencing. *Nat. Neurosci.* 24, 176–185.
 23. Wamstad, J.A., Corcoran, C.M., Keating, A.M., and Bardwell, V.J. (2008). Role of the transcriptional corepressor Bcor in embryonic stem cell differentiation and early embryonic development. *PLoS One* 3, e2814.
 24. Astolfi, A., Fiore, M., Melchionda, F., Indio, V., Bertuccio, S.N., and Pession, A. (2019). BCOR involvement in cancer. *Epigenomics* 11, 835–855.
 25. Ragge, N., Isidor, B., Bitoun, P., Odent, S., Giurgea, I., Cogné, B., Deb, W., Vincent, M., Le Gall, J., Morton, J., et al. (2019). Expanding the phenotype of the X-linked BCOR microphthalmia syndromes. *Hum. Genet.* 138, 1051–1069.
 26. Karczewski, K.J., Francioli, L.C., Tiao, G., Cummings, B.B., Alfoldi, J., Wang, Q., Collins, R.L., Laricchia, K.M., Ganna, A., Birnbaum, D.P., et al. (2021). Author Correction: the mutational constraint spectrum quantified from variation in 141,456 humans. *Nature* 590, E53.
 27. Stark, Z., Foulger, R.E., Williams, E., Thompson, B.A., Patel, C., Lunke, S., Snow, C., Leong, I.U.S., Puzriakova, A., Daugherty, L.C., et al. (2021). Scaling national and international improvement in virtual gene panel curation via a collaborative approach to discordance resolution. *Am. J. Hum. Genet.* 108, 1551–1557.
 28. Martinelli, S., Krumbach, O.H.F., Pantaleoni, F., Coppola, S., Amin, E., Pannone, L., Nouri, K., Farina, L., Dvorsky, R., Lepri, F., et al. (2018). Functional dysregulation of CDC42 causes diverse developmental phenotypes. *Am. J. Hum. Genet.* 102, 309–320.
 29. Reis, L.M., Tyler, R.C., Schilter, K.F., Abdul-Rahman, O., Innis, J.W., Koziel, B.A., Schneider, A.S., Bardakjian, T.M., Lose, E.J., Martin, D.M., et al. (2011). BMP4 loss-of-function mutations in developmental eye disorders including SHORT syndrome. *Hum. Genet.* 130, 495–504.
 30. van Paassen, B.W., van der Kooi, A.J., van Spaendonck-Zwarts, K.Y., Verhamme, C., Baas, F., and de Visser, M. (2014). PMP22 related neuropathies: charcot-Marie-Tooth disease type 1A and Hereditary Neuropathy with liability to Pressure Palsies. *Orphanet J. Rare Dis.* 9, 38.
 31. Carosso, G.A., Boukas, L., Augustin, J.J., Nguyen, H.N., Winer, B.L., Cannon, G.H., Robertson, J.D., Zhang, L., Hansen, K.D., Goff, L.A., and Bjornsson, H.T. (2019). Precocious neuronal differentiation and disrupted oxygen responses in Kabuki syndrome. *JCI Insight* 4, e129375. <https://doi.org/10.1172/jci.insight.129375>.
 32. Räsänen, N., Tiihonen, J., Koskivi, M., Lehtonen, Š., and Koistinaho, J. (2022). The iPSC perspective on schizophrenia. *Trends Neurosci.* 45, 8–26.
 33. Paulsen, B., Velasco, S., Kedaigle, A.J., Pigoni, M., Quadrato, G., Deo, A.J., Adiconis, X., Uzquiano, A., Sartore, R., Yang, S.M., et al. (2022). Autism genes converge on asynchronous development of shared neuron classes. *Nature* 602, 268–273.
 34. Wright, C.F., Fitzgerald, T.W., Jones, W.D., Clayton, S., McRae, J.F., van Kogelenberg, M., King, D.A., Ambridge, K., Barrett, D.M., Bayzina, T., et al. (2015). Genetic diagnosis of developmental disorders in the DDD study: a scalable analysis of genome-wide research data. *Lancet* 385, 1305–1314.
 35. Tate, J.G., Bamford, S., Jubb, H.C., Sondka, Z., Beare, D.M., Bindal, N., Boutselakis, H., Cole, C.G., Creatore, C., Dawson, E., et al. (2019). COSMIC: the catalogue of somatic mutations in cancer. *Nucleic Acids Res.* 47, D941–D947.
 36. Martin, A.R., Williams, E., Foulger, R.E., Leigh, S., Daugherty, L.C., Niblock, O., Leong, I.U.S., Smith, K.R., Gerasimenko, O., Haraldsdottir, E., et al. (2019). PanelApp crowdsources expert knowledge to establish consensus diagnostic gene panels. *Nat. Genet.* 51, 1560–1565.
 37. Ochoa, D., Hercules, A., Carmona, M., Suveges, D., Gonzalez-Uriarte, A., Malangone, C., Miranda, A., Fumis, L., Carvalho-Silva, D., Spitzer, M., et al. (2021). Open Targets Platform: supporting systematic drug-target identification and prioritisation. *Nucleic Acids Res.* 49, D1302–D1310.
 38. Merkle, F.T., Ghosh, S., Genovese, G., Handsaker, R.E., Kashin, S., Karczewski, K., O’Dushlaine, C., Pato, C., Pato, M., MacArthur, D.G., et al. (2020). Biological insights from the whole genome analysis of human embryonic stem cells. Preprint at bioRxiv. <https://doi.org/10.1101/2020.10.26.337352>.
 39. Amir, H., Touboul, T., Sabatini, K., Chhabra, D., Garitaonandia, I., Loring, J.F., Morey, R., and Laurent, L.C. (2017). Spontaneous single-copy loss of TP53 in human embryonic stem cells markedly increases cell proliferation and survival. *Stem Cell.* 35, 872–885.
 40. Rouhani, F., Kumasaka, N., de Brito, M.C., Bradley, A., Vallier, L., and Gaffney, D. (2014). Genetic background drives transcriptional variation in human induced pluripotent stem cells. *PLoS Genet.* 10, e1004432.
 41. Merkle, F.T., Ghosh, S., Genovese, G., Handsaker, R.E., Kashin, S., Meyer, D., Karczewski, K.J., O’Dushlaine, C., Pato, C., Pato, M., et al. (2022). Whole-genome analysis of human embryonic stem cells enables rational line selection based on genetic variation. *Cell Stem Cell* 29, 472–486.e7.
 42. Deciphering Developmental Disorders Study (2017). Prevalence and architecture of de novo mutations in developmental disorders. *Nature* 542, 433–438.
 43. Singh, T., Poterba, T., Curtis, D., Akil, H., Al Eissa, M., Barchas, J.D., Bass, N., Bigdeli, T.B., Breen, G., Bromet, E.J., et al. (2022). Rare coding variants in ten genes confer substantial risk for schizophrenia. *Nature* 604, 509–516.
 44. Gudmundsson, S., Singer-Berk, M., Watts, N.A., Phu, W., Goodrich, J.K., Solomonson, M., Genome Aggregation Database Consortium; Rehm, H.L., MacArthur, D.G., and O’Donnell-Luria, A. (2021). Variant interpretation using population databases: lessons from gnomAD. Preprint at arXiv. <https://doi.org/10.48550/arXiv.2107.11458>.
 45. Ruijtenberg, S., and van den Heuvel, S. (2016). Coordinating cell proliferation and differentiation: antagonism between cell cycle regulators and cell type-specific gene expression. *Cell Cycle* 15, 196–212. <https://doi.org/10.1080/15384101.2015.1120925>.
 46. Liu, L., Michowski, W., Kolodziejczyk, A., and Sicinski, P. (2019). The cell cycle in stem cell proliferation, pluripotency and differentiation. *Nat. Cell Biol.* 21, 1060–1067.
 47. Mitchell, J.M., Nemes, J., Ghosh, S., and Handsaker, R.E. (2020). Mapping genetic effects on cellular phenotypes with “cell villages”. Preprint at bioRxiv. <https://doi.org/10.1101/2020.06.29.174383>.
 48. Eichmüller, O.L., Corsini, N.S., Vértessy, Á., Morassut, I., Scholl, T., Gruber, V.-E., Peer, A.M., Chu, J., Novatchkova, M., Hainfellner, J.A., et al. (2022).

- Amplification of human interneuron progenitors promotes brain tumors and neurological defects. *Science* 375, eabf5546.
49. McLaren, W., Gil, L., Hunt, S.E., Riat, H.S., Ritchie, G.R.S., Thormann, A., Flicek, P., and Cunningham, F. (2016). The Ensembl variant effect predictor. *Genome Biol.* 17, 122.
 50. Danecek, P., and McCarthy, S.A. (2017). BCFtools/csq: haplotype-aware variant consequences. *Bioinformatics* 33, 2037–2039.
 51. Kang, H.M., Subramaniam, M., Targ, S., Nguyen, M., Maliskova, L., McCarthy, E., Wan, E., Wong, S., Byrnes, L., Lanata, C.M., et al. (2018). Multiplexed droplet single-cell RNA-sequencing using natural genetic variation. *Nat. Biotechnol.* 36, 89–94.
 52. Butler, A., Hoffman, P., Smibert, P., Papalexi, E., and Satija, R. (2018). Integrating single-cell transcriptomic data across different conditions, technologies, and species. *Nat. Biotechnol.* 36, 411–420.
 53. Falcon, S., and Gentleman, R. (2007). Using GOstats to test gene lists for GO term association. *Bioinformatics* 23, 257–258.
 54. Korsunsky, I., Millard, N., Fan, J., Slowikowski, K., Zhang, F., Wei, K., Baglaenko, Y., Brenner, M., Loh, P.-R., and Raychaudhuri, S. (2019). Fast, sensitive and accurate integration of single-cell data with Harmony. *Nat. Methods* 16, 1289–1296.
 55. Liberzon, A., Birger, C., Thorvaldsdóttir, H., Ghandi, M., Mesirov, J.P., and Tamayo, P. (2015). The Molecular Signatures Database (MSigDB) hallmark gene set collection. *Cell Syst.* 1, 417–425.
 56. 1000 Genomes Project Consortium; Abecasis, G.R., Auton, A., Brooks, L.D., DePristo, M.A., Durbin, R.M., Handsaker, R.E., Kang, H.M., Marth, G.T., and McVean, G.A. (2012). An integrated map of genetic variation from 1,092 human genomes. *Nature* 491, 56–65. <https://doi.org/10.1038/nature11632>.
 57. Lek, M., Karczewski, K.J., Minikel, E.V., Samocha, K.E., Banks, E., Fennell, T., O'Donnell-Luria, A.H., Ware, J.S., Hill, A.J., Cummings, B.B., et al. (2016). Analysis of protein-coding genetic variation in 60,706 humans. *Nature* 536, 285–291.
 58. Rentzsch, P., Witten, D., Cooper, G.M., Shendure, J., and Kircher, M. (2019). CADD: predicting the deleteriousness of variants throughout the human genome. *Nucleic Acids Res.* 47, D886–D894.
 59. Wolf, F.A., Angerer, P., and Theis, F.J. (2018). SCANPY: large-scale single-cell gene expression data analysis. *Genome Biol.* 19, 15.

STAR★METHODS

KEY RESOURCES TABLE

REAGENT or RESOURCE	SOURCE	IDENTIFIER
Deposited data		
Pooled dopaminergic differentiation	Jerber et al. ⁸	HipSci Managed access (EGA: EGAS00001002885) HipSci Open Access (ENA: ERP121676)
Whole exome sequencing (WES) of HipSci lines	HipSci Project https://www.hipsci.org	HipSci Managed access: EGA HipSci Open Access (ENA: ERP006946)
HipSci genotype array data	HipSci Project https://www.hipsci.org Kilpinen et al. ⁷	HipSci Managed access (EGA: EGAS00001000866, EGA: EGAS00001001272) HipSci Open Access (ENA: PRJEB11750)
Metadata for the dopaminergic differentiation single-cell dataset	This paper	https://zenodo.org/record/6079122#.YISkxNPMJhE (Open Access)
Processed single-cell count (dopaminergic differentiation) for days 11, 30 and 52.	This paper	https://zenodo.org/record/6079122#.YISkxNPMJhE (Open Access)
Macrophage differentiation	Alasoo et al. ¹³	Table S1
Sensory neuron differentiation	Schwartzentruber et al. ¹⁴	Table S1
Endoderm differentiation	Cuomo et al. ¹⁵	EGA:EGAS00001002278 EGA: EGAD0001005741 ENA:ERP016000
Somatic mutations (acquired <i>in vitro</i>)	Rouhani et al. ¹¹	https://doi.org/10.1101/2021.02.04.429731
Software and algorithms		
Variant effect predictor (VEP, release 99)	McLaren et al. ⁴⁹	https://www.ensembl.org/info/docs/tools/vep/index.html
BCFtools (version 1.4.25)	Danecek et al. ⁵⁰	https://samtools.github.io/bcftools/bcftools.html
Scanpy toolkit	Wolf et al. ⁵¹	https://scanpy.readthedocs.io/en/stable/
Cellranger v3.1.0	10x Genomics	https://support.10xgenomics.com/single-cell-gene-expression/software/downloads/latest
R (4.0.4) / Bioconductor (3.12)	R Core Team, 2021 Bioconductor Project, 2021	https://www.r-project.org/ https://www.bioconductor.org/
Seurat (v4.0.1)	Butler et al. ⁵²	https://satijalab.org/seurat/
GOstats (v2.56)	Falcon and Gentleman ⁵³	https://bioconductor.org/packages/release/bioc/html/GOstats.html
Harmony	Korsunsky et al. ⁵⁴	https://portals.broadinstitute.org/harmony/articles/quickstart.html
Demuxlet	Kang et al. ⁵¹	https://github.com/statgen/demuxlet
Other		
Human reference genome NCBI build 37, GRCh37	Genome Reference Consortium	http://www.ncbi.nlm.nih.gov/projects/genome/assembly/grc/human/
Developmental disorder genes (DDG2P, version 2.2)	Wright et al. ³⁴	https://nhsgms-panelapp.genomicsengland.co.uk/panels/484/v2.2
Cosmic database (cancer-associated genes, version 90 – GRCh37)	Tate et al. ³⁵	https://cancer.sanger.ac.uk/cosmic
MSigDB hallmark gene set signatures	Liberzon et al. ⁵⁵	https://www.gsea-msigdb.org/gsea/msigdb/
1000 Genomes Project	The 1000 Genomes Project Consortium et al. ⁵⁶	https://www.internationalgenome.org/
Exome Aggregation Consortium 0.3.1	Lek et al. ⁵⁷	https://gnomad.broadinstitute.org/downloads
CADD Phred scores (version 1.6)	Rentzsch et al. ⁵⁸	https://cadd.gs.washington.edu/score
Original code (Zenodo)	This paper	https://doi.org/10.5281/zenodo.7641259 (Open Access, frozen repository)

RESOURCE AVAILABILITY

Lead contact

Further information and requests for resources should be directed to and will be fulfilled by the lead contact, Helena Kilpinen (helena.kilpinen@helsinki.fi).

Materials availability

This study did not generate new unique reagents or new human iPSC lines.

Data and code availability

Exome sequencing from the HipSci project (www.hipsci.org) is available for both the parental fibroblasts and the iPSC lines (raw data). Data for the open access samples is deposited in the European Nucleotide Archive under study accession number (ENA: ERP006946). It includes 325 iPSC lines, of which 260 are also available for the parental fibroblasts. WES data for the managed access samples is deposited in the European Genotype-Phenotype Archive (EGA, <https://ega-archive.org>), with normal and specific disease cohort datasets available upon request and data access agreement. The variant call sets of acquired mutations *in vitro* and the code used to generate them are available at Rouhani et al.¹¹

As for the single-cell data from the iPSC dopaminergic differentiation, managed access data is available in the European Genome-phenome Archive (EGA: EGAS00001002885), as part of the EGAD00001006157 dataset. Open access samples are available in the European Nucleotide Archive (ENA: ERP121676) from the project PREJB38269. Metadata information for 828,937 processed cells from the DA dataset and AnnData/H5AD files containing the single-cell expression for days 11, 30 and 52 that are related to the STAR Methods are publicly available at Zenodo, <https://zenodo.org/record/6079122#.YISkxNPMJhE>. Chip genotypes for HipSci lines are available from the EGA (EGAS00001000866, EGAS00001001272) and the ENA (PRJEB11750) portals.

All original code is publicly available in a frozen Zenodo repository (<https://doi.org/10.5281/zenodo.7641259>). The repository includes the single-cell processing scripts, the downstream analysis, and the code to reproduce the main figures and the supplemental ones.

METHOD DETAILS

Somatic mutations acquired *in vitro* (SMAV)

A joint variant calling (BCFtools/mpileup and BCFtools/call, version 1.4.25, human genome assembly GRCh37d5) between 384 pairs of parental fibroblasts and their corresponding iPSC lines (251 donors) was performed to identify 18,999 somatic mutations that were acquired or positively selected throughout iPSC reprogramming as described in Rouhani et al.¹¹ This calling was performed for single-nucleotide variants (SNVs), dinucleotides, indels and copy number variants (CNVs) for both autosomal chromosomes and chromosome X. Only in the case of indels, chromosome X was not included.

We filtered the initial call set¹¹ following these steps: the variants out of the exome sequencing baits were excluded, germline variants were filtered-out assuming they show a minor allele frequency $MAF > 0.1\%$ in 1000 Genomes Phase3⁵⁶ or in ExAC 0.3.1,⁵⁷ or be carried by the parental fibroblast of more than one donor. Only high-quality variants were filtered-in (PASS filter). Variants with an allelic fraction larger than 0.6 in iPSC or in fibroblasts were removed to filter potential spurious mutation calls. We classified variants either as acquired *in vitro* or positively selected only when a significant rise in allele frequency was observed between the iPSC and the parental fibroblast (Fisher's exact test $p < 1.6 \cdot 10^{-4}$, equivalent to FDR 5% using the Benjamini-Hochberg multiple test correction procedure). 17 out of the 384 iPSC lines were found to be hypermutated *in vitro* (>240 mutations corresponding to a Z-score > 2) and were discarded for further analysis downstream. Finally, we defined our gene universe as the 19,653 genes that were protein-coding genes in the Ensembl gene annotation (GRCh37, version 87) and were covered by the exome sequencing baits. In line with that, we discarded all those variants that could not be annotated to the gene universe, finally releasing a call set of 18,999 mutations, including 460 CNVs, 642 indels, 2,445 dinucleotides and 15,452 SNVs (Table S1).

Functional annotation of SMAV

We annotated the somatic mutations acquired *in vivo* (SNVs, dinucleotides and indels from the 384 pairs of iPSC lines and their corresponding parental fibroblasts, $n=251$ donors) by predicting their functional consequence using the variant effect predictor⁴⁹ (VEP, release 99) and the haplotype-aware BCFtools/csq tool⁵⁰ (version 1.9). We used Ensembl gene annotations (GRCh37, version 87) and recorded only the most impactful consequence for each mutation, as determined by the following decreasing order of severity: https://www.ensembl.org/info/genome/variation/prediction/predicted_data.html.

We defined mutations as loss-of-function (LoF) when they were annotated as frameshift, stop-gain, splice acceptor or splice donor variants; and as missense pathogenic (or damaging missense) when annotated as missense or start loss with a CADD⁵⁸ Phred score cutoff > 15 (version 1.6). The definition of deleterious mutations included the union of LoF and missense pathogenic mutations. The remaining mutations were annotated as synonymous or as "others" (either as coding, non-coding or unannotated). Overall, we annotated 1,002 LoF mutations, 5,722 missense pathogenic, 2,631 missense non-pathogenic, 3,158 synonymous and 6,026 other mutations (Table S1).

Differentiation outcome of iPSC-derived cell types

Sensory neurons

We processed the [Table S1](#) of the original publication¹⁴ (“IPSDSNs”) that contained the metadata for all cell lines differentiated to sensory neurons. We annotated the differentiation outcome by re-labelling the neuron quality status per line from “Poor” to failed and from “Good” to successful. We excluded those cell lines with undefined neuron quality status and renamed the non-neuronal differentiation outcome to failed differentiation. We identified 13 iPSC lines with differentiation replicates, all of which had a concordant outcome (2 failed, 10 successful), except for one line (“HPSI0613i-eojr_3”) that was discarded. In total, we annotated the outcome for 105 cell lines (5 failed and 100 successful), of which 85 lines (3 failed, 82 successful) had also WES data for the parental fibroblasts (N=83 donors) ([Table S1](#)).

Macrophages

We processed the [Table S1](#) of the original publication¹³ that contained the status of the differentiation outcome per line. We removed those cell lines that showed a low macrophage purity (“FC_QC_fail”) or presented degraded RNA (“RNA_QC_fail”). We identified 11 iPSC lines with differentiation replicates, all of which had a concordant outcome (7 failed, 4 successful). In total, we annotated the outcome for 123 cell lines (23 failed and 90 successful), of which 102 lines (22 failed, 80 successful) had also WES data for the parental fibroblasts (N=102 donors) ([Table S1](#)).

Dopaminergic neurons

We reprocessed the whole scRNA-seq dataset (excluding cells treated with rotenone), re-clustering all cells at once and annotating the resulting cell types using the same markers from the original publication⁸ (see also [Reanalysis of pooled single-cell data](#)). We then computed the total number of cells and the cell type proportion per line in each pool. For each time point, we removed those cell lines with the lowest number of cells (first twentile) to increase the confidence level of the cell type proportion estimates. We then defined the neuronal differentiation efficiency per cell line in each pool as the proportion of dopaminergic and serotonergic neurons observed at day 52 of the differentiation. We annotated this efficiency for 209 cell lines distributed in 18 pools, and classified lines accordingly either as failed lines (<0.2, this includes lines with poor/impaired outcome) or successful lines (≥ 0.2). Only 3 out of the 36 iPSC lines placed in more than one pool (pool replicates) were discordant. The DA outcomes for the remaining 206 lines corresponded to 56 failed and 150 successful lines, of which a subset of 126 lines (35 failed, 91 successful) had also WES data for the parental fibroblasts (N=126 donors). Overall, we reached a 98.8% agreement with the neuronal differentiation outcome classification of the original paper.

Additionally, we processed the [Table S5](#) from Jerber et al.⁸ which contained the model scores from the predicted efficiency. Those scores were obtained from a logistic regression trained with a binary outcome definition per line (either successful lines with >20% measured efficiency or failed lines with <20%) and an independent dataset of bulk RNA-seq that uses all expressed genes from 184 iPSC lines. The model scores classified 812 HipSci iPSC lines as failed (N=103) and successful (N=709) differentiators (precision=0.9 and recall=0.35 for threshold=0.02231), of which 349 lines (33 failed, 316 successful) had also WES data for the parental fibroblasts (N=231 donors) (see [Figure 1A](#), [Table S1](#)).

Endoderm

We processed a table obtained from the authors of the original publication¹⁵ with the differentiation efficiency for 108 lines, of which 86 also had WES data for the parental fibroblasts. Here, differentiation efficiency is computed as the average pseudotime on day 3, having a continuous distribution of efficiencies rather than a binary outcome (“failed”, “successful”).

Gene burden differences upon differentiation outcome

We leveraged the 832 iPSC lines (from 547 donors) profiled with WES available from the HipSci project and annotated the most severe consequence for each variant using the variant effect predictor⁴⁹ (VEP, release 99) and the Ensembl gene annotation from the release (version 75). We summarise the results by building a matrix of mutation counts per variant category either for LoF or deleterious mutations representing gene damage categories, or synonymous variants as mutational burden control. The inclusion criteria in each of the variant categories was the same as provided with the annotation of somatic acquired mutations *in vivo* (see [Functional annotation of SMAV](#)). Each matrix contained the 19,653 genes (of the gene universe) as rows and the 832 lines as columns.

We then combined the mutational burden data per line for each variant category (LoF, deleterious and synonymous) with the corresponding binary differentiation outcome (DA predicted (N=793 lines from 529 donors), DA observed (N=183 lines, one line per donor), macrophages (N=118 lines, one line per donor)). We excluded the sensory neurons from the analysis due to the low number of failed lines in that dataset (N=3). For each variant category and outcome combination, we performed a Wilcoxon Rank Sum Test per gene (N=19,653 tests) to identify those that presented a differential burden between failed and successful lines. For each combination, we performed a multiple test correction using the Benjamini & Hochberg approach. The level of statistical significance was set at FDR=5%. To compute a fold change of the mutational differences per gene between failed and successful lines, we initially normalised the mutation ratio by the gene length (as in Ensembl Annotation release 87) and the number of lines per outcome and divided the ratios using pseudocounts. The pseudocounts used for each combination corresponded to the minimum non-zero normalised mutation rate observed across all genes for any of the outcomes. We used a threshold of $FC > 2.5$ or $FC < 1/2.5$ to classify genes as disproportionately mutated in failed lines or in successful lines, respectively. Alternatively in the case of the DA dataset, we also combined the burden data with the continuous distribution of differentiation efficiencies (N=183 lines) and predicted scores (N=793 lines) to check the robustness of the *BCOR* association. In this case, we performed a Pearson’s correlation per gene for each combination.

GO enrichment analysis (mutational burden)

For the gene ontology enrichment analysis on biological processes, we only focused on the deleterious burden of iPSC lines. Given the number of lines for the DA differentiation (183 lines for the observed outcomes, one line per donor: 48 failed vs 135 successful; and 793 lines for the predicted ones from 529 donors: 99 failed vs 694 successful), it is the variant category linked to gene damage with the best power to detect enrichment. We proceeded with the matrix of counts previously generated for the identification of gene burden differences linked to the differentiation outcome. Likewise, we computed the fold change of mutational differences per gene between failed and successful lines using the ratio of the mutation burden (mutations per Kb) normalised by gene length, number of lines per outcome and adding 0.001 as pseudocounts. Prior to the GO analysis, we annotated all genes with their corresponding Entrez gene identifiers and selected the most differentially mutated genes in successful lines (top-10% in \log_2FC) and the most differentially mutated in failed lines (bottom-10% in \log_2FC). We then run the hypergeometric test for GO term overrepresentation of biological processes conditional to the hierarchical GO structure (package *GOstats*⁵³ from R). For each of the four tests, we provided the selected genes in each DA outcome combination: failed/observed, failed/predicted, successful/observed and successful/predicted. We used the following thresholds: the cutoff for significance was set at $p < 0.05$, we considered only those gene sets defined with more than 20 genes and each gene set had to account for at least 10 counts in each analysis. All gene sets found to be significantly enriched are shown in [Table S3](#). Finally, we highlighted only those significant GO terms related to neurodevelopment or chromatin modification, so we highlighted any gene set with the following words in [Figure 2D](#): “Axon”, “neuron”, “glial”, “brain”, “hindbrain”, “forebrain”, “midbrain”, “synapse”, “chromatin”, “cerebellum”, “neural”, “cortex”, “neurogenesis”, “axonogenesis”, “nervous”, “hippocampus”, “neurotransmitter”, “dopaminergic”, “axenome”, “action potential” and “synaptic”.

Reanalysis of pooled single-cell data (DA)

Sample selection and data pre-processing

The dopaminergic neuron differentiation was profiled by droplet-based scRNA-seq (10x Genomics). We processed a subset of the dopaminergic neuron differentiation dataset⁸ that consisted of 119 10x samples out of the total 166 ([Table S5](#)). Here, a 10x sample is defined as the cells sequenced from one inlet of a 10x chip. For the sake of this study, we did not include those samples from the original experiment profiled under rotenone treatment at day 52 or containing iPSC-derived cerebral organoids (day 119). We also did not process samples for pool 10 (day 11) with reported problems on library preparation. We processed the 119 10x samples using Cell Ranger software (version 3.1.0) and aligned them to the GRCh37/hg19 reference genome. Gene counts were quantified by the “count” option of the software, using the Ensembl 87 reference gene annotation (N=32,738 genes). After pre-processing, we excluded 4 additional 10x samples due to quality control issues, mainly due to low percentages of cell singletons in deconvolution ($\leq 50\%$) and low cell viability: two technical replicates from pool 12 on day 52, one sample from pool 8 on day 30 and a sample from pool 1 on day 30 ([Figure S2B](#)). The final 115 10x samples covered all pooled experiments (N=19, pools 1-17 and pools 20-21), including 238 different cell lines (230 donors, 7-24 lines per pool). Only one cell line (“HPSI0913i-gedo_33”) was previously removed due to an abnormally high cell line proportion ($>90\%$) in pool 14.

Quality control and deconvolution of cell donor identity

Each 10x sample went through a quality control step in which we removed dying cells or those with broken membranes, displaying a low number of genes per cell (<200) and an excess of mitochondrial count fraction ($>5\%$). Also, we discarded those cells with an abnormal percentage of reads consumed by the top-100 mostly expressed genes ($<75\%$), which indicate technical artefacts compromising the coverage of the full transcriptome of the cells. On the other hand, we filtered out those genes that were not expressed in at least 0.1% of the total cells.

For each of the 19 pools, we performed cell deconvolution using *demuxlet*⁵¹ using existing genetic variation (genotypes of common biallelic exonic variants, $MAF > 5\%$) available from the HipSci Project⁷ as in the original paper. In those cases when iPSC cell lines had not been genotyped (intended cell lines from [Table S4](#)), we used the genotypes from the primary fibroblast instead when available. Demuxlet was run using a default prior doublet rate of 0.5. We only retained those (singletons) cells that could unambiguously be linked to a donor and discarded those 10x samples for which the overall singleton outcome was low ($<50\%$) ([Figure S2B](#)). After deconvolution, 236 (n=228 donors) out of the 238 lines of the experiment had at least one cell detected. We performed the quality control and the integration of the 10x samples using the Scanpy Python-based toolkit⁵⁹ (version 1.4.5.1).

Normalisation, dimensionality reduction, batch correction and clustering

We performed a combined analysis of all the three time points (day 11, day 30 and day 52) to have a shared embedding for all 236 lines. Initially, genes that were not expressed in at least 0.1% of total cells were removed. Then, gene counts were normalised to the total number of counts per cell and log-transformed (\log_1p). After adjusting for mean-variance dependence, we selected the 2,928 highly variable genes and scaled gene counts to unit variance and zero mean. We then calculated the first 50 principal components (PCs) and batch-corrected them with Harmony,⁵⁴ treating each 10x sample as a different batch (parameters: $\theta = 2$, $\text{max.iter.harmony} = 25$, $\text{max.iter.cluster} = 500$). We then used the batch-transformed PCs to compute a neighbourhood graph ($n_neighbors = 10$), visualise it using UMAP and perform the cell clustering using the Leiden algorithm (resolutionN=0.3) identifying 12 different clusters ([Figures S2H–S2J](#)). We also used the Scanpy toolkit (version 1.4.5.1) for all the steps, except for Harmony that was run in R version 4.0.3.

Cell type annotation

Cell type annotation was performed using the same set of literature-curated markers as in Jerber et al.⁸ ([Figures S2E–S2G](#) and [Table S6](#)). We confidently annotated 10 out of the 12 identified clusters. Interestingly, we could also identify neuroblasts at day 11

with a commitment to dopaminergic neurons, as they clustered together, but at the same time did not exhibit the neuron marker expression.

At day 11, we characterised four populations of floor-plate midbrain progenitors, either proliferating (proFPP-1, proFPP-2) or non-proliferating (FPP-1, FPP-3). We could also link the population of neuroblasts to their early dopaminergic or serotonergic commitment. At day 30 and 52, we identified six additional cell types, including another cell type of non-proliferating progenitors (FPP-2), two neuronal populations (dopaminergic-like (DA) and serotonergic-like (Sert-like) neurons) and three non-neuronal ones (astrocytes (Astro), ependymal-like cells (Epend-1) and an unknown population (Unk-1) potentially linked to Cajal-Retzius transient neurons. At day 30, two additional rare cell types (<2%) were identified, either belonging to a subgroup of Sert-like neurons associated with proliferation markers (pro.Sert-like), or to an unknown population (Unk-2) only detected in a single 10x sample of pool 12.

Pool reproducibility of cell line abundance

We started processing the metadata object containing annotations from all cells (available online, see [Data and code availability](#)). To define different types of replicates, we used the information provided by the metadata of the 115 10x samples ([Table S5](#)). Four replicate types were defined per cell line ([Figure S3C](#)).

- **Pool replicates** (41 cell lines, N=90 replicate comparisons): The same cell line was placed in different pooled experiments (different cell lines in the background).
- **Biological replicates** (31 cell lines, N=31 replicate comparisons): One cell line underwent independent differentiations (different time and plate), but within the same pool (same background).
- **Technical replicates** (200 cell lines, N=644 replicate comparisons): One cell line underwent differentiation within the same pool, same time, but different wells of the same plate.
- **10x replicates** (109 cell lines, N=699 replicate comparisons): One cell line underwent differentiation within the same pool, same time and same well of the plate.

Initially, we calculated the cell line proportion within each 10X sample. Then, for each cell line, the corresponding replicate group and a given time-point, we calculated the averaged cell line proportion per replicate taking into account the contributing 10X samples. For instance, to compare the cell line proportion of the two biological replicates for “HPS11014i-tuju_1” at day 11, we averaged the cell line proportion of the four 10X samples contributing to replicate 1 on one side, and the four 10x samples contributing to replicate 2, on the other. To evaluate the reproducibility between replicate proportions, we fitted a linear regression and computed the adjusted R-squared and the p-value of the association. Data points on [Figure 3C](#) correspond to matched replicates per line/time-point combination. Note here that the designation of replicate 1 or replicate 2 before the regression is random.

Cell line proliferation in DA differentiation

The cell suspension for each pool was prepared with an equal amount of each iPSC line.⁹ For this analysis, we only considered those cell lines within a given pool that had been sampled in the three time points of the differentiation (N=164 cell lines used in 187 pool/line combinations, one cell line per donor). For each pool and time-point, we computed the log-transformed (log1p) cell line proportion. Then, we calculated the proliferation rate at day 11, day 30 and day 52, dividing the cell line proportions observed at each respective time point by the equal proportions from day 0. We then annotated each cell line with the observed outcome in the DA dataset, either successful or failed, based on the neuron differentiation efficiency threshold of 0.2. Additionally, we annotated failed cell lines with either *BCOR*+ (N=20) or *BCOR*- (N=30) based on the presence of LOF *BCOR* variants in each line. Note here that none of the successful lines (N=114) carried any LoF mutation in our iPSC exome-sequencing data.

Annotation of cancer-driver mutations

For each of the 832 iPSC cell lines with exome sequencing data, we annotated the most severe consequence for each variant using the variant effect predictor (VEP, release 99) as described earlier (see [Functional annotation of SMAV](#)). We then overlapped the predicted LoF variants from each line with those listed in the database for the cancer-associated genes (Cosmic Tier 1, version 94) under the strongest evidence for oncogenic activity (Tier 1). We restricted the overlap search to those Cosmic Tier 1 variants that have a defined genomic position and a FATHMM¹¹ score ≥ 0.7 . We identified 726 potential driver mutations with 606 iPSC lines carrying at least one driver mutation. The most mutated driver genes were *PDE4DIP* (564), *CCND3* (35), *TCF3* (29) and the *BCOR* (24), also after normalising the burden by the CDS length. We then annotated each cell line with both the observed (183 lines, 48 failed and 135 successful) and predicted DA differentiation (793 lines from 529 donors: 99 failed and 694 successful) and computed the driver mutational ratio (log2-transformed) given the outcome. In both cases, *BCOR* ranked as the gene with the highest ratio of driver mutations in failed lines versus successful ones (5:0 with the observed DA outcome, 17:6 with the predicted DA outcome).

Differential abundance analysis

After annotating the cell type, we used the metadata information for each cell to compute the cell type proportions per line (available online, see [Data and code availability](#)). We used the outcome annotation for the 206 lines classified either as failed or successful, as described for dopaminergic neurons. For 8 pool replicates missing day 52 time-point in one of the pools, we imputed the same

outcome as observed in the other replicate. We also included 15 out of the 18 lines that were not profiled at day 52, but with data from previous time-points (either from day 11 or 30, or from both). To take advantage of those lines in the cell type composition analysis, we classified them either as successful or failed using the predicted model scores from Jerber et al.⁸ Following those steps, we end up annotating the differentiation outcome for 221 lines (58 failed, 163 successful) from 214 donors.

For each time-point and cell type, we used a negative binomial regression model to evaluate the composition changes between failed and successful lines. We modelled the total number of cells per line as an offset variable, given that the accuracy of cell type proportion estimates increases with their magnitude.

$$\text{glm.nb}(\text{ncells} \sim \text{outcome} + \text{offset}(\log(\text{nTotalCells})))$$

We finally performed a multiple-test correction (N=36 tests) using the Benjamini & Hochberg approach (FDR<5%). The significance level of the mean cell type proportion difference between mutated and unmutated groups is indicated by different levels: pAdj<0.05 (*), pAdj<0.01 (**), pAdj<0.001 (***).

Impact of deleterious burden in *BCOR*

We considered 141 iPSC lines (one line per donor) with these available information layers: cell type proportion estimates on day 52 (see [Differentiation outcomes of iPSC-derived cell types](#)), *in vitro* proliferation rates (see [Cell line proliferation in DA differentiation](#)) and deleterious burden (see [Gene burden differences upon the differentiation outcome](#)). For each gene (N=19,653), we compared the cell type composition differences at the end of the differentiation between those lines carrying at least one deleterious mutation and those lines unmutated (Wilcoxon Rank Sum Test). For each cell type, we applied multiple-test correction (Benjamini & Hochberg, FDR<5%) to the raw p-values obtained from each gene and indicated whether they are more abundant in mutated (blue) or unmutated lines (orange). Note here that only those cell types that show >2% of abundance at day 52 were considered, discarding FPP-1, FPP-3, proliferative serotonergic-like neurons, proliferative FPP-2 and the unknown cell type 2.

Alternatively, for each major cell type at day 52 (>2% abundance), we tested for the association between cell type proportions per line and their corresponding proliferation rates between day 52 and day 0, using Pearson's correlation (N=154 lines, one line per donor). We corrected for multiple-test correction using the Benjamini & Hochberg method (N=7 major cell types, FDR<5%). We also indicated if the cell type proportions correlate (blue) or anti-correlate (orange) in [Figure 4B](#). The significance level of all comparisons was indicated as follows: pAdj<0.05 (*), pAdj<0.01 (**), pAdj<0.001 (***).

DE analysis between failed and successful lines

We leveraged the gene expression data from 221 lines (214 donors) annotated with the DA outcome (58 failed, 163 successful), see [Differential abundance analysis](#). Overall, we processed 273,804, 266,226 and 306,811 cells from day 11, day 30 and day 52, respectively. For each time-point, we load the "AnnData/H5AD" object with the unscaled log-transformed gene expression per cell (available online, see [Data and code availability](#)) and filtered out those genes expressed in less than 1% of the cells, finally processing 12,912, 14,149 and 14,737 genes, respectively. We performed differential gene expression analysis between failed and successful lines for each cell type and time point combination using the Wilcoxon Rank Sum test (as implemented in Seurat⁵²). We required more than 10 cells to be represented in each of the outcomes to run the DE test for each combination. DE genes were selected based on an adjusted P-value < 0.05 and a FC > 1.5.

For each cell type and time point, we also tested the overrepresentation of three gene sets (Cosmic-Tier1, DDD and a subset of dominant DDD genes) among the list of DE genes (Chi-squared test using p-values computed by Monte Carlo simulation using 100,000 replicates). The employed gene universe consists of the union of pass-filtered genes across all time points (N=15,367). We corrected for multiple-test correction using the Benjamini & Hochberg method (N=102, FDR<5%). The significance level of each test was indicated as follows: pAdj<0.05 (*), pAdj<0.01 (**), pAdj<0.001 (***).

GO enrichment analysis (gene expression)

We performed 12 gene ontology enrichment tests on biological processes based on.

- The union of genes found to be differentially expressed in any given time point and cell type combination (labeled **allIDE**).
- The union of genes found to be differentially expressed in any given time point and cell type combination with an overrepresentation of DDD DE genes (labeled **signifDDD**).
- The lists of DE genes for each of the 10 time point and cell type **combinations** with an overrepresentation of DDD DE genes (cyan circles with p<0.05, [Figure 4C](#)).

Previous to the GO analysis, we annotated each feature of the gene universe (N=15,367) with their corresponding Entrez gene identifiers using the package *org.Hs.eg.db* from R/Bioconductor. We discarded from the analysis those genes without correspondence or showing duplicate identifiers. We then run the hypergeometric test for GO term overrepresentation of biological processes conditional to the hierarchical GO structure (package *GOstats*⁵³ from R). Given the different magnitude of DE genes between **allIDE** (N=1,884) or **signifDDD** (N=972) and each of the combination tests (N=131-372), we used different thresholds for significance in each case: **allIDE/signifDDD**: {minimum gene set size = 30, maximum gene set size=200, pAdj<0.001, minimum number of counts

per gene set = 20); **combinations:** {minimum gene set size = 10, maximum gene set size=200, pAdj<0.001, minimum number of counts per gene set = 7}.

All gene sets found to be significantly enriched are shown in [Table S7](#). Finally, we highlighted only those significant GO terms related to neurodevelopment or chromatin modification, so we highlighted any gene set with the following words in [Figure 4D](#): “Axon”, “neuron”, “glial”, “brain”, “hindbrain”, “forebrain”, “midbrain”, “synapse”, “chromatin”, “cerebellum”, “neural”, “cortex”, “neurogenesis”, “axonogenesis”, “nervous”, “hippocampus”, “neurotransmitter”, “dopaminergic”, “axenome”, “action potential” and “synaptic”.

Gene set enrichment analysis (cancer genes)

We performed a gene set enrichment analysis (GSEA) on those time point and cell type combinations in which the list of differentially expressed genes were enriched in cancer-associated genes. For this purpose, we used the curated MSigDB hallmark gene set signatures (version 7.4 for symbol identifiers).⁵⁵ We considered only those gene sets with a larger size than 10 genes. For each gene set, we then ran the preranked gene set enrichment analysis with a maximum gene set size of 500 genes, an eps parameter of 0 and used 10,000 permutations for preliminary estimation of p-values. We highlighted significantly enriched gene sets as those with a BH-adjusted p-value < 0.05 and an enrichment score normalised to mean enrichment of random samples of the same size (NES): NES ≥ 1.5 for upregulated pathways and NES ≤ -1.5 for downregulated ones.

Outlier lines in cell type composition

We calculated the cell type fraction per line within each pool and time point, removing those lines with the lowest number of cells (first twentile, 227 lines from 219 donors). Those cell lines pooled in more than one experiment (pool replicates) were treated as independent lines (N=272 combinations). We then computed the z-score associated with the calculated fractions and marked as outliers those lines showing a cell type fraction with a |Z-score|>2, either showing a deficiency or an excess of a given cell type.

We characterised the outlier behaviour focusing on those cell lines represented in the three time points of the differentiation (112 lines, 121 pool-line combinations). Based on that, we computed the number of times each line shows an abnormal cell type fraction (outlier event) throughout the entire differentiation or specifically per time point (bars represent 95% confidence interval in [Figure 5B](#), top-left). For each cell line, we explored when outlier events occurred and identified the most common time point combinations.

For those lines profiled with WES for the iPSC and the corresponding parental fibroblasts, we annotated the burden of somatic acquired mutations *in vivo* ([Table S1](#)) considering either total or deleterious variants. We then evaluated whether cell lines defined as outliers of cell type composition (91 lines, 103 pool-line combinations) showed mean differences on the mutational burden (Wilcoxon Rank Sum Test) to the non-outliers (N=57 lines, 60 pool-line combinations). Alternatively, we also evaluated the outlier lines within each specific time point.

Finally, we also annotated each cell line with their corresponding proliferation rate at day 52 (see [Cell line proliferation in DA differentiation](#)) and fitted a logistic regression to predict the outlieriness of cell type composition (N=159 lines, 182 pool-line combinations).

Gene expression and cell type abundance links

We analysed the correlation between the cell type abundance and the cell-type-specific expression for all genes using the existing cell line variability throughout the differentiation (N=236 lines from 228 donors). We computed the z-scores for cell type composition as in *Outlier lines in cell type composition*. As for the gene expression (log_{1p} normalised counts, not-scaled), we computed the z-score per cell type using the average gene expression per line at each time point. The average gene expression per line was calculated considering all the cells of that given line in one specific pool experiment (N=281 combinations), including those from different 10x samples when available. We required a minimum of 10 cells per line (in any time point - cell type combination) to calculate the average gene expression. We discarded all those combinations in which less than 10 lines matched this threshold (proliferative Sertoli-like neurons at day 11 and the glial cells (Unk-2) at days 11 and 52).

We then correlated the expression z-scores with the cell type fraction z-scores, as shown in the example for *KMT2D* gene for DA and FPP-1 in day 11 ([Figure 5D](#)). To identify the key genes driving the outlieriness in cell type composition, we performed the z-score correlations for all the detected genes per time point (day 11, N=12,912; day30, N=14,149; day 52, N=14,737). Those genes with no detectable expression in at least 10 lines of a given combination were not considered. We then sampled the genes with either positive or negative significant associations (p.Adj<0.05) from the resulting distribution of Pearson correlation coefficients per cell type ([Figure 5D](#), lower).

From the list of genes with significant correlation (or anti-correlation) per cell type and time point, we tested whether there was a gene set enrichment on several panels of genetic disease associations: developmental disorder genes³⁴ (DDD), cancer-associated genes³⁵ (Cosmic-Tier1), schizophrenia³⁷ (Open Targets Platform), and three panels from Genomics England:³⁶ adult onset neurodegenerative disorder (Panel App v2.178), bleeding and platelet disorders (v1.2) and family pulmonary fibrosis (v1.29). We performed an hypergeometric test for overrepresentation considering the list of significantly and non-significantly correlated genes and the overlap with each gene set and cell type separately. We then performed multiple-test correction using the Benjamini & Hochberg method (N=198 tests, FDR<5%). The significance level of each test was indicated as follows: pAdj>0.05 (ns), pAdj<0.05 (*), pAdj<0.01 (**), pAdj<0.001 (***)

Cell Genomics, Volume 3

Supplemental information

**Somatic mutations alter the differentiation
outcomes of iPSC-derived neurons**

Pau Puigdevall, Julie Jerber, Petr Danecek, Sergi Castellano, and Helena Kilpinen

Supplemental Figures

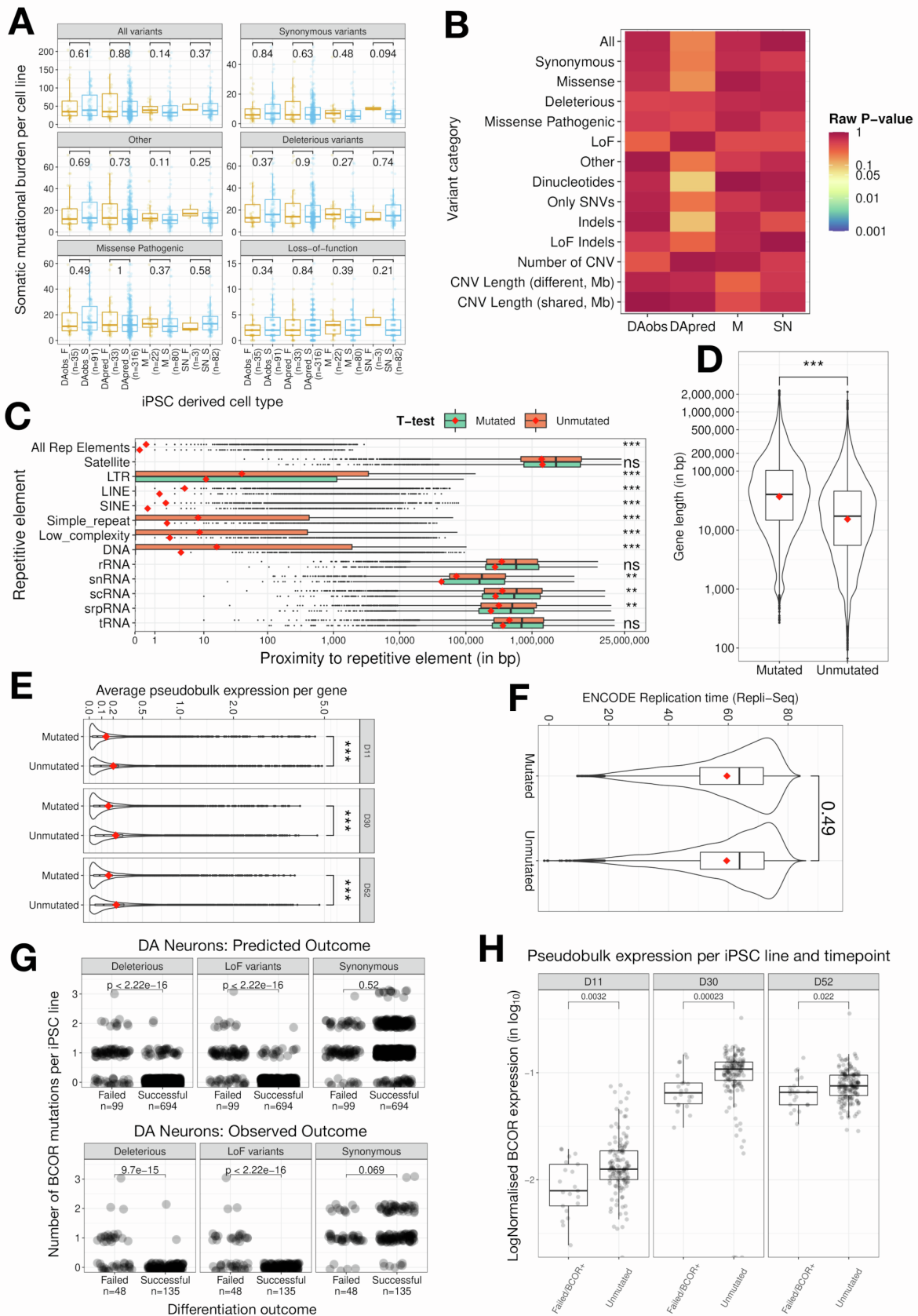


Figure S1. Total somatic burden did not alter the differentiation outcome, but LoF mutations in *BCOR* compromised neuron production and gene expression. Related to Figures 2A-2B.

(A) No significant mean differences on total number of mutations acquired *in vitro* (Wilcox.test, FDR<5%) were observed between the two differentiation outcomes (failed vs successful) of the three different iPSC-derived cell types (dopaminergic neurons - observed and predicted-, macrophages and sensory neurons). We also tested such differences of burden on six variant classes: total variants excluding CNVs; synonymous variants and others (coding, non-coding and unannotated), deleterious variants (union of LoF and missense pathogenic), as well missense pathogenic and loss-of-function variants alone. In none of the 24 tests, the difference reached the statistical significance threshold, even before multiple test-correction.

(B) No association was observed between the binary differentiation outcome (failed or successful groups) and the total number of mutations acquired *in vitro* for any of the tested variant classes. For each mutation category, we fitted a logistic regression and showed the corresponding raw p-values shown in the heatmap. None of the tests reached the statistical significance threshold even before multiple-test correction. We considered all mutations (without CNVs), synonymous, missense (pathogenic and non-pathogenic), deleterious and LoF only, other mutations (coding, non-coding and unannotated), dinucleotides, single nucleotide variants only, indels, indels predicted to be LoF, the number of CNVs, and the region length (in Mb) of shared and different CNVs.

(C) Genes with acquired somatic mutations in our dataset (n=9,235) showed a significantly closer proximity to repetitive elements (UCSC RepeatMasker [S2]) than unmutated genes (n=11,118), except for satellite repeats, ribosomal RNA and transfer RNA (T-test, pAdj<0.05).

(D) Mutated genes were longer on average than unmutated genes (T-test, $p < 1.02 \cdot 10^{-149}$).

(E) Mutated genes showed reduced expression when compared with unmutated genes (T-test, $p < 0.05$). Gene expression values were calculated from the average pseudobulk log-normalised values per line and time point.

(F) Genes with somatic acquired mutations did not show differences on replication timing when compared to unmutated genes (T-test, $p = 0.49$). Previously, each gene was annotated with an average replication timing (Wavelet-smoothed signal) from the ENCODE Repli-seq BG02ES ESC line [S3]. The average was computed across all the signal values from the 1-Kb windows overlapping each corresponding gene.

(G) Number of *BCOR* mutations per iPSC line (either LoF, deleterious or synonymous variants) linked to the DA differentiation outcome (observed and predicted). A significant higher burden of damaging variants were observed across failed lines (Wilcox.test, $p < 0.05$). None of the successful lines (N=135) in the DA observed outcome carried a *BCOR* LoF mutation, while 22 out of 48 failed lines have at least one mutation.

(H) Failed lines in DA differentiation with LoF mutations in the *BCOR* gene show significantly reduced *BCOR* expression when compared with unmutated lines, either failed or successful (Wilcox.test, $p < 0.05$). Expression units correspond to pseudobulk log-normalised values per iPSC line and time point.

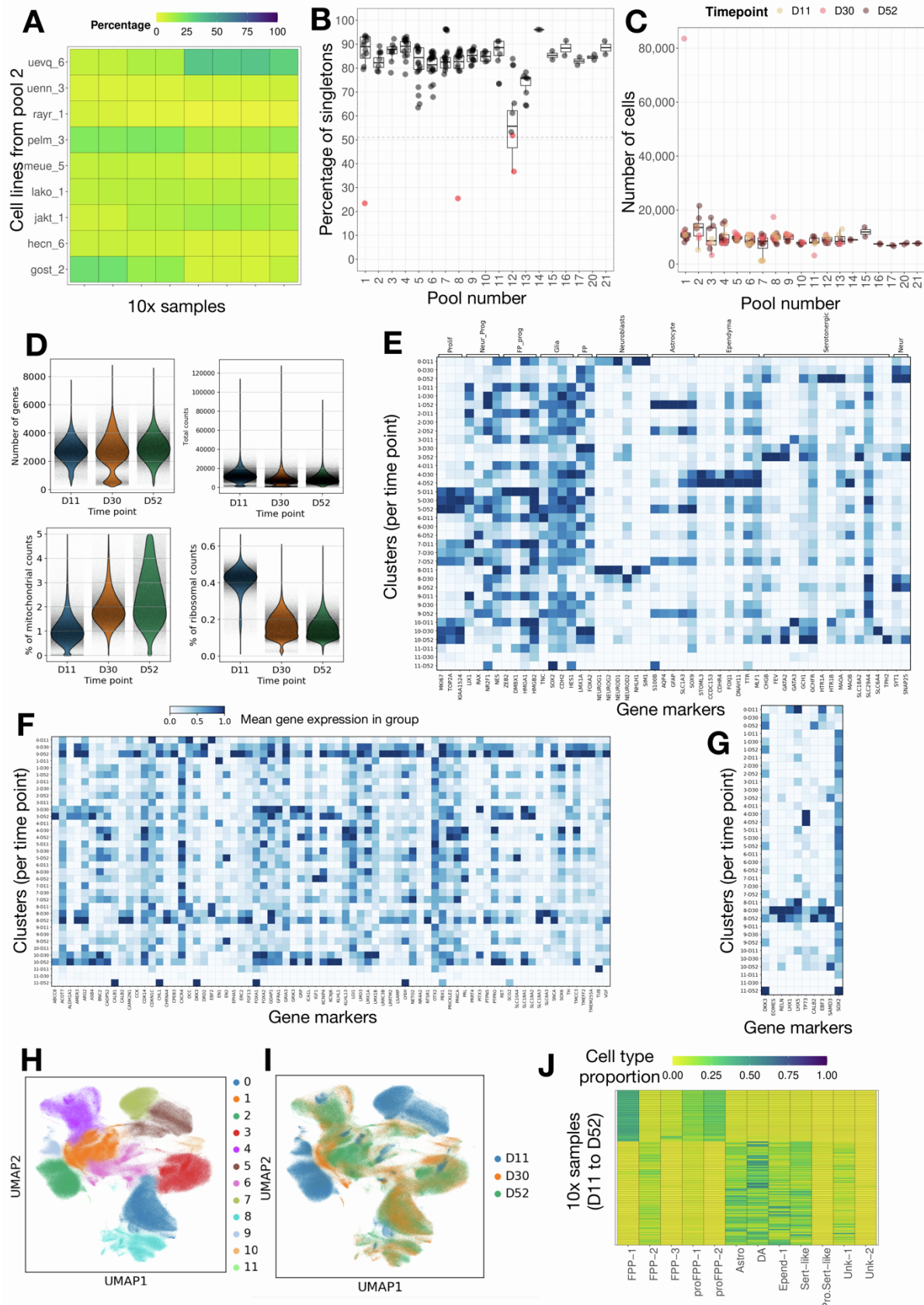


Figure S2. Quality control and annotation of the pooled DA differentiation dataset. Related to Figures 3A and 4A.

(A) Cell line proportion for the different 10x samples run for pool 2. Each heatmap row is a cell line and each column corresponds to a 10x sample. In certain samples, one-to-two cell lines consistently account for up to 50% of the cells.

(B) Percentage of singletons confidently assigned to a 10x sample (each dot) of day 52 grouped by pool. As a quality control step, those 10x samples with less than a 50% of singletons were removed from further analysis due to concerns on data integrity.

(C) Number of cell droplets estimated per 10x sample after CellRanger processing.

(D) Quality control metrics after the merging and the cell deconvolution of the 115 10x samples from the dopaminergic differentiation. The median number of genes per cell was below 3,000, while the total count of reads was around 10,000, as expected. Also, cells at day 52 showed a higher average of mitochondrial counts, while at day 11 the higher percentage corresponded to ribosomal counts.

(E-G), Time-specific cell markers expression from Julie et al [S1] used to annotate our Leiden clustering. General markers are shown in (E), specific dopaminergic markers in (F) and glial cells in (G). The intensity of blue shows the mean expression of the gene for each cluster-time point group.

(H) UMAP based on gene expression with cells coloured by the annotated cell types.

(I) UMAP on gene expression with cells coloured by sampling time point in differentiation (days 11, 30 and 52).

(J) Cell type proportion in each 10x sample highlights the observed variability on cell type composition throughout differentiation. Each row is a 10x sample ordered by time point, without considering the contribution of individual lines.

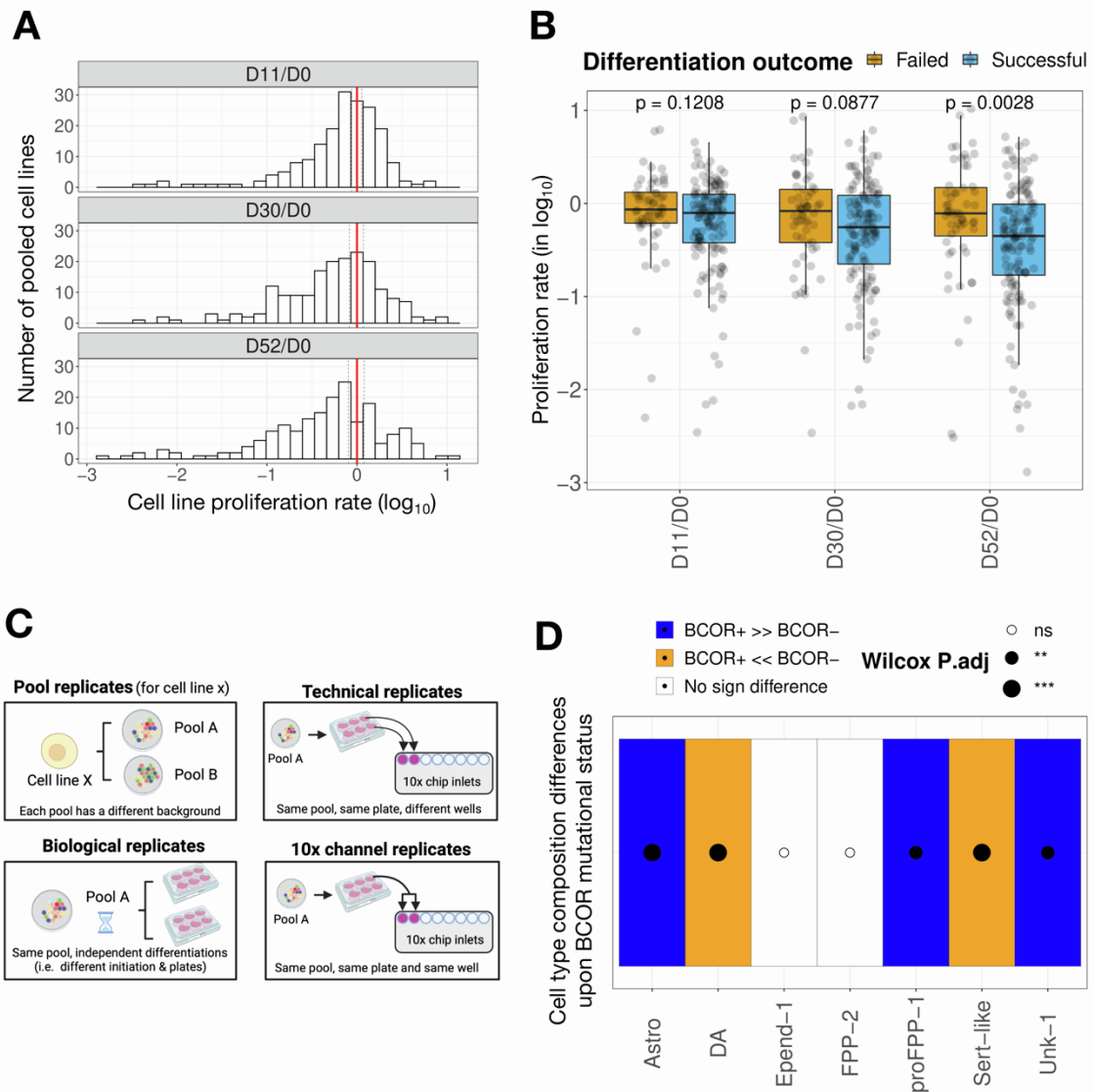


Figure S3. Differentiation failure is driven by increased proliferation rate and *BCOR* LoF mutations. Related to Figures 3B-3C and 4B.

(A) Distribution of the *in vitro* proliferation rate for pooled cell lines (expressed in \log_{10}) between each differentiation time point and day 0. The vertical red line indicates the mean cell line proportion ratio and the dashed lines the 95% confidence intervals.

(B) Failed cell lines showed on average a larger proliferation rate at day 52 than successful lines (Wilcoxon Rank Sum Test, $p=2.8 \cdot 10^{-3}$). Proliferation rates are expressed in \log_{10} values.

(C) Illustrative diagram for the four types of replicates considered in DA dataset: pool replicates, referred to cell lines that are included in different pools; biological replicates, referred to lines from the same pool that are differentiated independently (in time and space); technical replicates, referred to lines from the same pool differentiated in the same plate but different wells; and 10x replicates, referred to lines from the same pool, plate and well.

(D) Cell lines carrying at least one deleterious *BCOR* mutation were associated with cell type composition changes at day 52 with a significant depletion of dopaminergic and serotonergic-like neurons (DA and Sert-like) and an excess of astrocytes (Astro), proliferative floor-plate progenitors type 1 (proFPP-1) and glial cells (Unk-1). The test for association was run for all protein-coding genes (Wilcoxon Rank Sum Test) and corrected for multiple-testing (Benjamini & Hochberg). The increasing size of the black-filled circle indicates higher significance levels for gene set enrichment: $p < 0.01$ (**), $p < 0.001$ (***); while the white-filled circles indicate non-significant association. Cell types with a significantly higher proportion in mutated lines compared to the unmutated ones are labelled in blue. In the opposite scenario, they are labelled in orange.

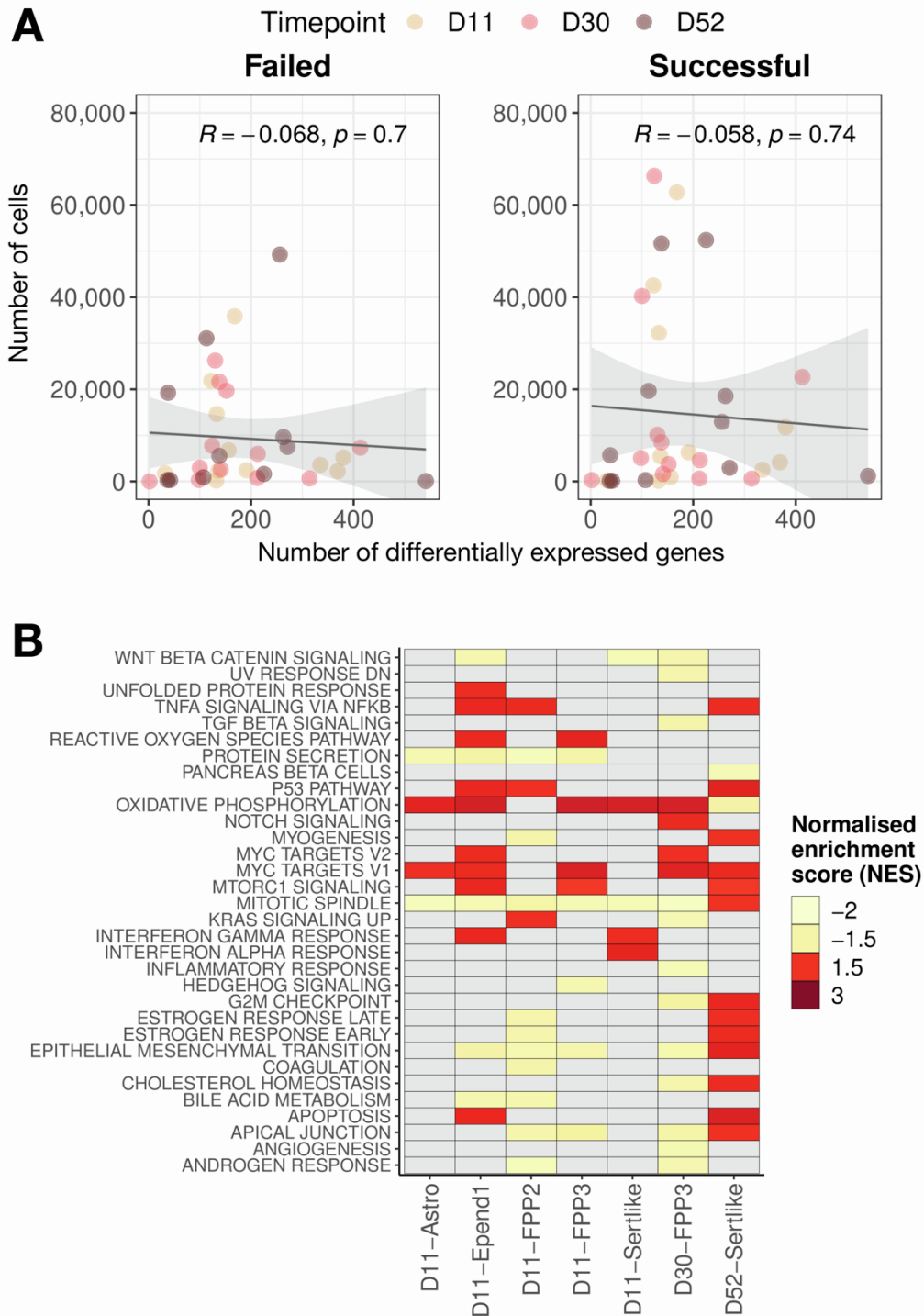


Figure S4. GSEA hallmark signatures for cell types with cancer-associated differential gene expression. Related to Figure 4C.

(A) Quality control: the number of cells per outcome and cell type did not correlate with the detected number of differentially expressed (DE) genes ($p > 0.05$), suggesting that differential gene expression was not biased by the sample sizes. Each dot represents a cell type and is coloured according to the corresponding time point.

(B) Gene set enrichment analysis on MSigDB hallmark signatures [S4] ($|NES| > 1.5$, $adj.P < 0.05$) among those cell types with cancer-associated differential gene expression. Pathways with significant enrichment are coloured in red for upregulation, in yellow for downregulation and in grey when no significant enrichment is observed. Astrocytes at day 52 downregulated the oxidative phosphorylation and upregulated the mitotic spindle assembly, contrary to other cell types.

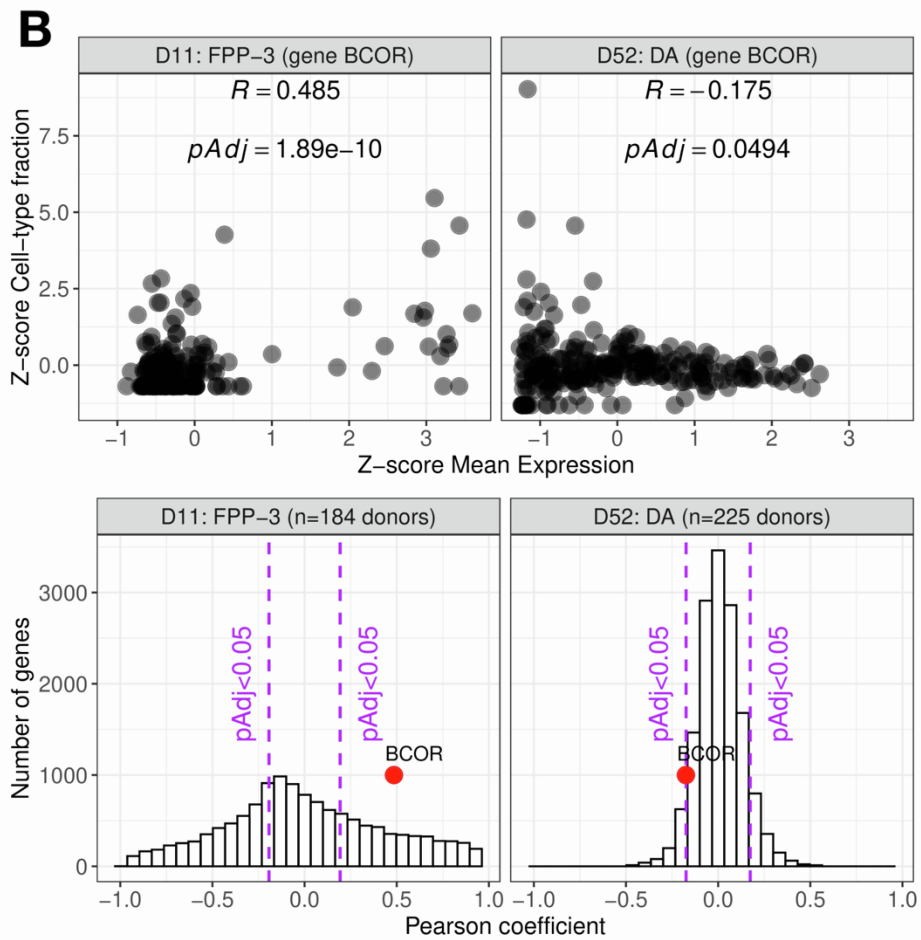
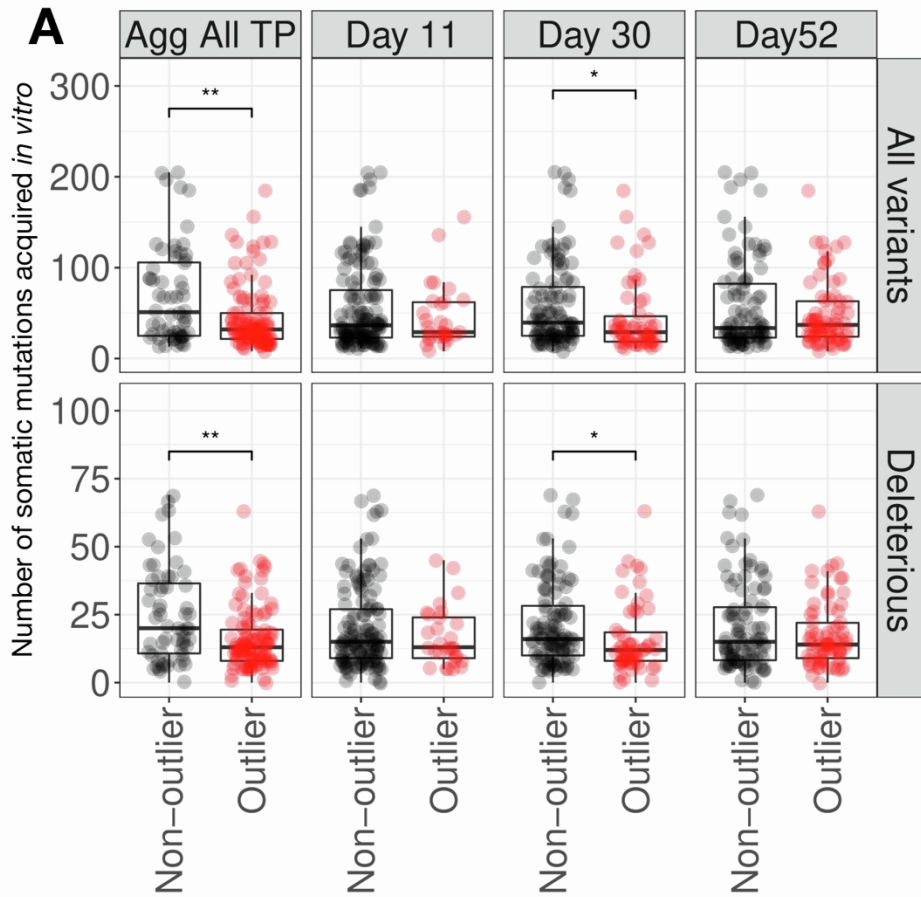


Figure S5. iPSC lines with outlier cell type composition showed reduced somatic burden only at day 30. Related to Figures 5B and 5D.

(A) The differences in the burden of somatic mutations acquired *in vitro* between outliers and non-outliers of cell type composition were not consistent throughout the different stages of the differentiation (Wilcox.test). The definition of outlier lines was based on the observation of an abnormal cell type proportion during the differentiation or at a given time point. Only at day 30, we observed a reduced burden in the outlier group, which was also observed with the aggregated definition, both when accounting for total mutations or for deleterious mutations only.

(B) upper: z-score correlation of gene expression (i.e *BCOR*) and cell type proportions of floor-plate progenitors type 3 (FPP-3) at day 11 and dopaminergic neurons (DA) at day 52. Each dot is an iPSC line; **lower:** The distribution of Pearson correlation coefficients for all genes expressed in previous cell types and time points. Point highlighted in red indicates where *BCOR* is in that distribution.

Supplemental References

- S1. Jerber, J., Seaton, D.D., Cuomo, A.S.E., Kumasaka, N., Haldane, J., Steer, J., Patel, M., Pearce, D., Andersson, M., Bonder, M.J., et al. (2021). Population-scale single-cell RNA-seq profiling across dopaminergic neuron differentiation. *Nat. Genet.* *53*, 304–312.
- S2. Jurka, J. (2000). Repbase update: a database and an electronic journal of repetitive elements. *Trends Genet.* *16*, 418–420.
- S3. Hansen, R.S., Thomas, S., Sandstrom, R., Canfield, T.K., Thurman, R.E., Weaver, M., Dorschner, M.O., Gartler, S.M., and Stamatoyannopoulos, J.A. (2010). Sequencing newly replicated DNA reveals widespread plasticity in human replication timing. *Proc. Natl. Acad. Sci. U. S. A.* *107*, 139–144.
- S4. Liberzon, A., Birger, C., Thorvaldsdóttir, H., Ghandi, M., Mesirov, J.P., and Tamayo, P. (2015). The Molecular Signatures Database (MSigDB) hallmark gene set collection. *Cell Syst* *1*, 417–425.